T.C.
NECMETTİN ERBAKAN UNIVERSITY
INSTITUTE OF SCIENCE

G-QUADRUPLEX STABILIZERS AS METABOLIC REGULATOR AND THERANOSTIC AGENT

Beyza BAŞAR

MASTER'S THESIS

Department of Molecular Biology and Genetics

July-2025
KONYA

THESIS APPROVAL AND ACCEPTANCE

The thesis study titled “G-Quadruplex Stabilizers as Metabolic Regulators and Theranostic Agents” prepared by Beyza BAŞAR has been accepted as a MASTER’S THESIS by the following jury on 03/07/2025 unanimously vote in the Department of Molecular Biology and Genetics of the Institute of Science at Necmettin Erbakan University.

Jury Members	**Signature**
Chair Assist. Prof. Fatma SEÇER ÇELIK	……..
Advisor Assoc. Prof. Dr. Sündüs ERBAŞ ÇAKMAK	……..
Member Assist. Prof. Tuğba Nur ASLAN	……..

Approved by the Institute of Science Administrative Board on …./…/20.. with the decision number ……..

Prof. Dr. Havvanur UÇBEYİAY
Institute Director

This thesis study was supported by TUBITAK 2247-A with project number 120C125 at Necmettin Erbakan University Science and Technology Research and Application Center (BITAM).

TEZ BİLDİRİMİ

Bu tezdeki bütün bilgilerin etik davranış ve akademik kurallar çerçevesinde elde edildiğini ve tez yazım kurallarına uygun olarak hazırlanan bu çalışmada bana ait olmayan her türlü ifade ve bilginin kaynağına eksiksiz atıf yapıldığını bildiririm.

DECLARATION PAGE

I hereby declare that all information in this document has been obtained and presented in accordance with academic rules and ethical conduct. I also declare that, as required by these rules and conduct, I have fully cited and referenced all material and results that are not original to this work.

Beyza BAŞAR

Tarih: 03.07.2025

ÖZET

YÜKSEK LİSANS TEZİ

METABOLİK REGÜLATÖR VE TERANOSTİK AJAN OLARAK G-KUADRUPLEKS STABİLİZATÖRLERİ

Beyza BAŞAR

Necmettin Erbakan Üniversitesi Fen Bilimleri Enstitüsü
Moleküler Biyoloji ve Genetik Anabilim Dalı

Danışman: Doç. Dr. Sündüs ERBAŞ ÇAKMAK

2025, 82 Sayfa

Jüri
Doç. Dr. Sündüs ERBAŞ ÇAKMAK
Dr. Öğretim Üyesi Tuğba Nur ASLAN
Dr. Öğretim Üyesi Fatma SEÇER ÇELİK

DNA, replikasyon, transkripsiyon gibi çeşitli metabolik süreçleri yönetmek için çift sarmal yapısını çözerek belirli koşullar altında kanonik katlanmış B-DNA yapısı yerine B olmayan farklı ikincil DNA konformasyonları oluşturabilmektedir. Bu yapılar arasında, G-kuadrupleks yapılar (G4'ler), düzenleyici elemanlar olarak hücresel metabolizmadaki önemli rolleri nedeniyle dikkat çekmiştir. Bu nedenle, G4 yapılarına odaklanılmış ve hücre üzerindeki etkileri üzerine birçok çalışma yürütülmüştür. İnsan genomunda 700.000'den fazla potansiyel G4 yapısının olduğu ve genom promotörlerinin %40'tan fazlasının G4 yapıları içerebileceği tahmin edilmektedir. G4 ligandları tarafından G4 promotör bölgelerinin stabilizasyonu ile onkogenlerin gen ifadesinin azaltılması, hücresel metabolizmanın düzensizliğine neden olarak apoptoza da yol açabilmektedir. Dahası, G4 stabilizasyonunun sağladığı genomik instabilite, helikaz aktivitesinin çalışmasını etkileyerek DNA hasarına neden olabilir. Bu nedenle, G-kuadrupleks yapıları kanser çalışmaları için potansiyel hedeftirler.

Bu tez çalışması kapsamında, onkogenlerin DNA G-kuadrupleks bölgelerine bağlanarak metabolik düzenleyici olarak görev yapan yapısında klorambusil alkilleme ilacı içeren (L1) ve ikili kapasiteye (hem terapötik hem de tanısal) sahip teranostik ajan (L2) olarak yeni G-kuadrupleks ligandları geliştirilmiştir. BODIPY düzlemsel ana gövdesine sahip bileşik L1, G4 bölgesine bağlanarak belirli onkogen ifadelerini düzenleyebilmiştir. Ayrıca, L1'in anti-metastatik etkisi, yara kapanmasının inhibe edildiği hücre göçü analizinde de gösterilmiştir. Teranostik ligand L2, floresan prob gibi G4 yapısına bağlandıktan sonra emisyonda bir değişikliğe neden olabilen iki floresan üniteye sahiptir. Bu bileşik, DNA G4 bölgesine bağlanmasına bağlı olarak hem emisyon değişimini hem de onkogen ifadesinin inhibisyonunu arttırabilmiştir. Tez çalışmasında elde edilen verilerin yeni nesil G4 ligandları olarak anti-kanser çalışmalarına katkı sunacağı düşünülmektedir.

Anahtar Kelimeler: G-kuadrupleks ligandları, teranostik ajanlar, kanser tedavileri, BODIPY

ABSTRACT

MS THESIS

G-QUADRUPLEX STABILIZERS AS METABOLIC REGULATORS AND THERANOSTIC AGENTS

Beyza BAŞAR

INSTITUTE OF SCIENCE

NECMETTİN ERBAKAN UNIVERSITY
THE DEGREE OF MASTER OF SCIENCE

Advisor: Assoc. Prof. Dr. Sündüs ERBAŞ ÇAKMAK

2025, 82 Pages

Jury
Assoc. Prof. Dr. Sündüs ERBAŞ ÇAKMAK
Assist. Prof. Dr. Tuğba Nur ASLAN
Assist. Prof. Dr. Fatma SEÇER ÇELİK

DNA canonical B-form double helix structure can be unwound and some secondary structures critical for the regulation of some metabolic processes such as replication and transcription can be generated. Among these structures, G-quadruplexes (G4s) have gained attention due to their key roles in cellular metabolism as regulatory elements. Therefore, G4 structures have been under focus and many studies have been conducted to understand their cellular roles. It is estimated that there are more than 700,000 potential G4 structures in the human genome, and more than 40% of genome promoters may contain G4 structures. Reduction of expression of oncogenes through stabilization of G4 promoter regions with the use of G4 ligands causes dysregulation of cellular metabolism resulting in apoptosis as well. Moreover, the genomic instability provided by G4 stabilization interferes with helicase activity and can induce DNA damage. Therefore, G-quadruplexes are potential target for cancer studies.

In this thesis study, novel G-quadruplex ligands were developed as chlorambucil bearing metabolic regulator (L1) and theranostic agent (L2) which has dual capacity (both therapeutic and diagnostic) upon binding DNA G-quadruplex regions of the oncogenes. Compound L1 with BODIPY planar backbone was able to suppress certain oncogene expressions through binding to G4 region. Furthermore, the anti-metastatic effect of L1 was also shown in cell migration assay where wound closure was significantly inhibited by the ligand. The theranostic ligand L2 has two fluorescent units that could cause a change in emission after binding to G4 structure like a fluorescent probe. This compound could have enhanced emission and inhibit oncogene expression after binding to DNA G4 region.

Keywords: G-quadruplex ligands, theranostic agents, oncogene expression, cancer treatments, BODIPY

ACKNOWLEDGEMENT

I would like to express my sincere gratitude to my supervisor Assoc. Prof. Dr. Sündüs ERBAŞ ÇAKMAK for her support, guidance, and motivation throughout my academic journey.

I would like to thank my lab mates Ayşe İlayda BOYACI, Aliye Beyza ÖZÇELİK, Betül ALTUNKAYNAK, Emin ŞAHİN, Hacer Ravza UÇAR and Dr. Safaa ALTVEŞ for their support and friendships. It was a great chance to work with them in this lab.

I would especially like to express my sincere gratitude to Prof. Dr. Mahmut Deniz YILMAZ who kindly answered my endless questions and encouraged me throughout my master's studies.

I would like to thank other members of SEC-LAB and YC-LAB for their share of knowledge and kindness. I would also like to thank to Dr. Fatma SEÇER ÇELİK for her contributions.

I would also like to thank my family and my friends who always support and believe me to achieve my goals. I could not have completed this journey without them. I will be deeply grateful, for the rest of my life, to my sister Esra who had given me all her love, belief and support throughout her life.

I would like to thank TÜBİTAK for the financial support provided to me through the TÜBİTAK BİDEB 2210-A National Graduate Scholarship Program during my master's studies. Also, TÜBİTAK 2247 (Grant No: 120C125) is acknowledged for the research involving L1 ligand.

Lastly, I would like to thank myself for finishing this thesis despite all the challenges along the way.

Beyza BAŞAR
KONYA-2025

TABLE OF CONTENTS

ÖZET ..... **iv**

ABSTRACT ..... **v**

ACKNOWLEDGEMENT ..... **vi**

TABLE OF CONTENTS ..... **vii**

1. INTRODUCTION **1**

2. LITERATURE REVIEW **2**

2.1. Alternative Structures of DNA 2
2.2. G-quadruplexes as Non-Canonical DNA Structure 3
2.3. The Relationship Between Cancer and G-quadruplexes 5
2.4. G-quadruplexes as Drug Targets in Cancer 6
2.4.1. Use of G4 ligand to target telomeres 7
2.4.2. Reduced oncogene expression by G4 ligands 8
2.4.3. G4 structures and genomic instability 8
2.5. G-quadruplex Ligands 9
2.6. G-quadruplex Ligands in Anti-Cancer Therapies as Regulators 10
2.7. Theranostic Agents 11
2.8. G-quadruplex Ligands with Theranostic Properties 11

3. MATERIALS AND METHODS **13**

3.1. Design, Synthesis and Characterization of Compounds 13
3.1.1. Design of ligand L1 13
3.1.2. Synthesis of compound 1 15
3.1.3. Synthesis of compound 2 16
3.1.4. Synthesis of compound 3 17
3.1.5. Synthesis of compound 4 18
3.1.6. Synthesis of compound 5 19
3.1.7. Synthesis of compound 6 20
3.1.8. Synthesis of compound L1 21
3.1.9. Design of ligand L2 22
3.1.10. Synthesis of compound 8 23
3.1.11. Synthesis of compound 9 24
3.1.12. Synthesis of compound 10 (L3) 25
3.1.13. Synthesis of compound 11 26
3.1.14. Synthesis of compound 12 27
3.1.15. Synthesis of compound L2 28
3.2. FRET Melting Assay 28
3.3. Emission Measurements of Theranostic Ligand (L2) 29
3.4. Cell Culture Experiments 30
3.4.1. Cellular cytotoxicity assay (MTT) 30

3.4.2. Cell migration assay 31
3.4.3. RNA extraction from cancer cells 31
3.5. Detection of Gene Expression Level (RT-PCR) 32
3.6. Analysis of DNA Alkylation by L1 34

4. RESULTS AND DISCUSSION 35

4.1. Synthesis of Compounds 35
4.2. FRET Melting Assay 35
4.3. Emission Measurements of Theranostic Ligand (L2) 37
4.4. Cell Culture Experiments 38
4.4.1. Cellular cytotoxicity assay (MTT) 38
4.4.2. Cell migration analysis 41
4.4.3. Analysis of gene expression 42
4.5. Detection of DNA Alkylation by L1 44

5. CONCLUSIONS AND RECOMMENDATIONS 46

5.1 Results 46
5.2 Recommendations 46

6. REFERENCES 47

APPENDIX 50

Appendix-1 ^{1}H NMR spectrum of compound 6 (400 MHz, $CDCl_3$) 50

Appendix-2 ^{13}C NMR Spectrum of compound 6 (101 MHz, $CDCl_3$). 51

Appendix-3 HRMS Spectrum of compound 6 52

Appendix-4 ^{1}H NMR spectrum of compound L1 (400 MHz, $CDCl_3$). 53

Appendix-5 ^{13}C NMR Spectrum of compound L1 (101 MHz, DMSO-d_6). 54

Appendix-6 HRMS Spectrum of compound L1 55

Appendix-7 ^{1}H NMR spectrum of compound 8 (400 MHz, $CDCl_3$) 56

Appendix-8 ^{13}C NMR Spectrum of compound 8 (101 MHz, $CDCl_3$). 57

Appendix-9 HRMS Spectrum of compound 8 58

Appendix-10 ^{1}H NMR spectrum of compound 9 (400 MHz, $CDCl_3$) 59

Appendix-11 ^{13}C NMR Spectrum of compound 9 (101 MHz, $CDCl_3$). 60

Appendix-12 HRMS Spectrum of compound 9 61

Appendix-13 ^{1}H NMR spectrum of compound 10 (400 MHz, $CDCl_3$) 62

Appendix-14 ^{13}C NMR Spectrum of compound 10 (101 MHz, $CDCl_3$). 63

Appendix-15 HRMS Spectrum of compound 10 64

Appendix-16 ^{1}H NMR spectrum of compound 11 (400 MHz, $CDCl_3$)..... 65

Appendix-17 ^{13}C NMR Spectrum of compound 11 (101 MHz, $CDCl_3$)..... 66

Appendix-18 HRMS Spectrum of compound 11 67

Appendix-19 ^{1}H NMR spectrum of compound 12 (400 MHz, $CDCl_3$)..... 68

Appendix-20 HRMS Spectrum of compound 12 69

Appendix-21 ^{1}H NMR spectrum of compound L2 (400 MHz, $CDCl_3$ 70

Appendix-22 HRMS Spectrum of compound L2 71

SYMBOLS AND ABBREVIATIONS

Symbols

mL:	milliliter
µL:	microliter
nm:	nanometer
µM:	micromolar
µm:	micrometer
mM:	millimolar
MHz:	Mega Hertz
kb:	kilobase
°C:	degree Celsius

Abbreviations

ANOVA: One-Way Analysis of Variance

B-actin: Beta-actin gene

BCL-2: B-cell lymphoma

BODIPY: 4,4-Difluoro-4-bora-3a, 4a-diaza-s-indacene (Boron dipyrromethene)

CDH-1: Cadherin-1

cDNA: complementary DNA

COX-4-2: Cytochrome c oxidase subunit 4 isoform 2

DCM: Dichloromethane

DNA: Deoxyribonucleic acid

dNTP: Deoxynucleotide triphosphate

DMF: Dimethylformamide

DMSO: Dimethyl sulfoxide

dsDNA: double-stranded DNA

FAM: 5(6)-Carboxyfluorescein

FBS: Fatal Bovine Serum

FRET: Förster Resonance Energy Transfer

ELISA: Enzyme-Linked Immunosorbent Assay

EtOAc: Ethyl Acetate

Et_3N: Triethylamine

GAPDH: Glyceraldehyde-3-phosphate dehydrogenase

G4: G-quadruplex

GLUT-1: Glucose transporter-1

HG-DMEM: High Glucose Dulbecco's Modified Eagle Medium

HIF-1: Hypoxia-Inducible Factor-1

HRMS: High Resolution Mass Spectrometry

H-TERT: Human telomerase reverse transcriptase

K_2CO_3: Potassium Carbonate

KIT: Receptor tyrosine kinase

KRAS: Kirsten Rat Sarcoma viral oncogene homolog

LiCl: Lithium Chloride

LiOH: Lithium Hydroxide

MeCN: Acetonitrile

MetOH: Methanol

MCF-7: Human breast cancer cell line (Michigan Cancer Foundation-7)

$MgCl_2$: Magnesium Chloride

mRNA: messenger ribonucleic acid

MTT: 3-(4,5-dimethylthiazol-2-yl)-2,5-diphenyltetrazolium bromide

MYC: Myelocytoma oncogene

Na_2SO_4: Sodium sulfate

NaN_3: Sodium azide

NIR: Near-Infrared

NMR: Nucleic Magnetic Resonance

PBS: Phosphate Saline Buffer

PCR: Polymerase Chain Reaction

PDK-1: 3-Phosphoinositide-dependent kinase 1

RT-qPCR: Reverse transcription-quantitative polymerase chain reaction

RNA: Ribonucleic acid

TAMRA: 5(6)-Carboxytetramethylrhodamine

THF: Tetrahydrofuran

TLC: Thin Layer Chromatography

UTR: Untranslated region

WNT-1: Wingless-type MMTV integration site family member 1

VEGF: Vascular Endothelial Growth Factor

1. INTRODUCTION

This thesis project aims to develop novel nucleic acid G-quadruplex ligands for specific binding to G-quadruplex regions of DNA. These regions can be found in many promoter regions of oncogenes. Therefore, these ligands are expected to bind G4 structures at promotor sites and cause decrease in expression of these oncogenes. There are two different ligands designed; compound L1 is a metabolic regulator which has DNA alkylation activity with anticancer agent chlorambucil and compound L2 is a theranostic agent which has therapeutic and diagnostic dual capability. In the literature, there are several G4 ligands but there is no distyryl pyridinium BODIPY G4 ligand structure conjugated to alkylating agent chlorambucil used as metabolic regulator or theranostic BODIPY-based G4 stabilizer. These change in the emission of the ligand can enable G4 binding while an accompanying gene regulation can be done.

2. LITERATURE REVIEW

The first attempt for understanding the chemical forms of genetic material was started the discovery of deoxyribonucleic acid in 1869 by Friedrich Miescher (Mirsky, 1968). Almost a century later, the right-handed double helix DNA structure, known as B-DNA, was resolved in 1953 by Watson and Crick by results of their X-ray diffraction studies. DNA generally exists as double-helix, which acts as the carrier of the genetic information., During metabolic processes (such as replication and transcription) the structure is denatured, and the DNA double helix is converted into locally a single-stranded sequence. These single strand sequences may contain repetitive sequences which can form non-B DNA conformations instead of canonical folded B-DNA under certain conditions (Choi & Majima, 2011). For example, Lyamichev et al. observed a structure as Hoogsteen paired triple DNA helix, and Wang et al. proposed the left-handed conformation of Z DNA in 1986 (Boyer, Grgurevic, Cazaux, & Hoffmann, 2013). Since then, several other non-B DNA secondary structures were discovered including hairpin, triplex (H-DNA), cruciform, tetraplex etc.

2.1. Alternative Structures of DNA

It is stated that the repeated sequences of DNA are more than 50% of total genome but simple sequence repeats comprise almost 3% of the total DNA. These repeats form certain structures as mentioned (hairpin, triplex (H-DNA), cruciform, junctions, tetraplex, G-quadruplexes etc.) are formed using non-canonical interactions, different than traditional B-DNA (Figure 2.1). Unusual base pairs such as Hoogsteen base pairs differ from Watson-Crick base pairing (AT, GC) instead G-G, C-C, or G-G-C pairing. On the other hand, the cruciform, Z-DNA and hairpin have stabilized by Watson–Crick base pairing even their structures are different from B-DNA. Moreover, not all the conformations are based on Watson-Crick base pairing, some of them have Hoogsteen type of base pairing in which non canonical hydrogen bonding occurs between some nucleic acids (e.g. G-G or C-C) (Choi & Majima, 2011).

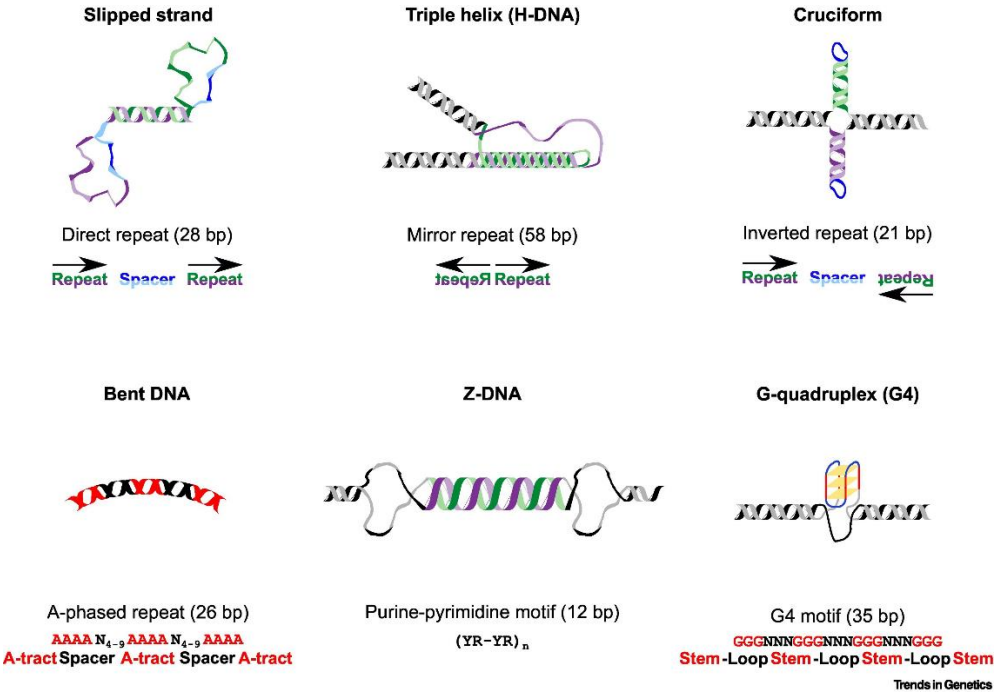

Figure 2.1. Non-B DNA conformations (Makova & Weissensteiner, 2023)

2.2. G-quadruplexes as Non-Canonical DNA Structure

Early studies of G-quadruplexes were started in 1910 when guanylic acid is found to form gel at high concentrations, which suggested that G-rich sequences in DNA may form higher-order structures. In 1962, Gellert et al. described that guanylic acid could form tetrameric structures (Gellert, Lipsett, & Davies, 1962) (Bochman, Paeschke, & Zakian, 2012). By 1987, Henderson and colleagues discovered the first G-quadruplex molecules in eukaryotic chromosomal telomeric DNA (Henderson, Hardin, Walk, Tinoco Jr, & Blackburn, 1987). G-quadruplexes are one of the non-canonical folded secondary structures of nucleic acids which has been found in guanine rich regions. They are formed by the π-π stacking of two or more guanine quartets (G-quartets) and each G-quartet is composed of four guanines in a square planar configuration connected by Hoogsteen type of base pairing. They are highly thermodynamically stable structures. The stability of G4 depends on topology, loop size and the base composition of G-quadruplexes (Mishra et al., 2019). Moreover, the stability of this quartet formation relies on monovalent metal cations such as Na^+ or K^+ (rarely Li^+) with the coordination of carbonyl oxygen O6 atoms of guanine bases. Since G-quadruplexes (G4s) are highly polymorphic structures, they

can form through inter or intramolecular folding (Figure 2.2). Depending on the orientation of the guanine bases on the DNA strand, these structures can be; parallel if in the same direction, anti-parallel if in the opposite direction, and hybrid if both the same and opposite strands are involved (Figueiredo, Mergny, & Cruz, 2024).

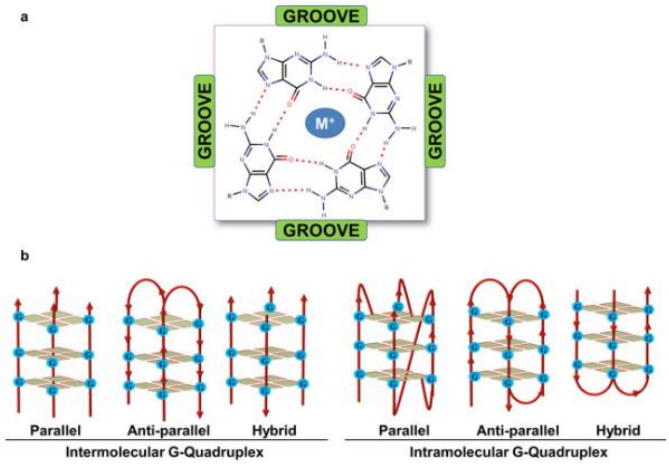

Figure 2.2. a) G-quartet structure **b)** Different topologies of G-quadruplex structures. M^+ represents any cation (Mishra, Jain et al. 2019)

Bioinformatics analysis demonstrated that human genome has over 700,000 G-quadruplex forming sequences. In fact, there are over 40% of human genome promoter have G4 structure itself. Interestingly, G4 locations are not randomly distributed throughout genome but instead they have been found in key sites of the genome such as telomeres, promoter regions, replication origins, 5' and 3' UTR of mRNA (Banerjee, Panda, & Chatterjee, 2022). For example, G4 formation can inhibit new DNA synthesis if located in replication fork. The RNA synthesis is also inhibited during transcription if the template strand contains the potential G4-containing sequence. On the other hand, if there is a possibility of G4 presence in coding strand, it may cause formation of RNA G4 sequence which can prevent transcription later. Therefore, G-quadruplexes have roles in many cellular processes including telomere maintenance, DNA replication, gene expression and mRNA translation as represented in Figure 2.3 (Nakanishi & Seimiya, 2020).

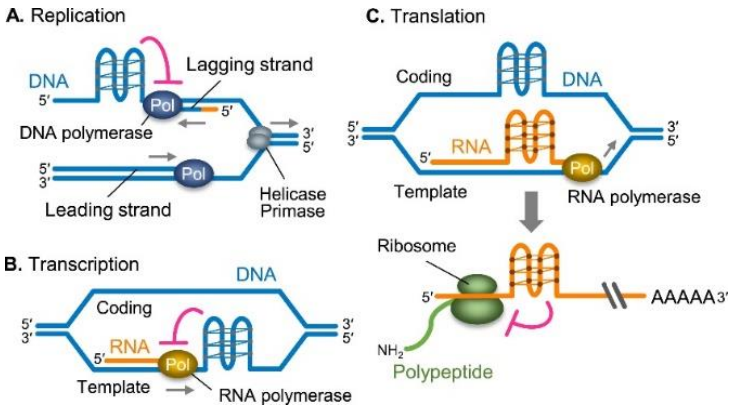

Figure 2.3. Possible involvement of G4s in various biological events (Nakanishi and Seimiya 2020)

2.3. The Relationship Between Cancer and G-quadruplexes

Since G-quadruplexes have been found in significant regulatory regions of the human genome, they interfere with a variety of biological processes, replication and transcriptional functions and other important processes associated with cancer (Sanchez-Martin, Lopez-Pujante, Soriano-Rodriguez, & Garcia-Salcedo, 2020). Therefore, G4s have great impact on biological metabolic pathways which become dysfunctional in diseases, such as cancer. Hence, there are several studies targeting G4s as a therapeutic application. As a result, cancer-related functions of G-quadruplexes pave the way for alternative therapeutic approaches in cancer (Brooks, Kendrick, & Hurley, 2010). Cancer is caused by uncontrollable cell division due to de-regulated processes during cancer development. There are six main cellular and biological processes which are considered as dysregulated during oncogenic transformation and malignancy. These are activation of replicative immortality, sustaining proliferative signalling, resistance to cell death, evasion of growth suppressors, induction of angiogenesis, tissue invasion and metastasis which constitute hallmarks of cancer. In each hallmark, certain critical genes have G-quadruplex structure in their core or proximal promoter sites. Genes associated with the hallmarks of cancer are shown in Figure 2.4 and they are classified according to their most common potential biological impacts. Some may even be involved in more than one hallmarks of cancer (Sanchez-Martin et al., 2020).

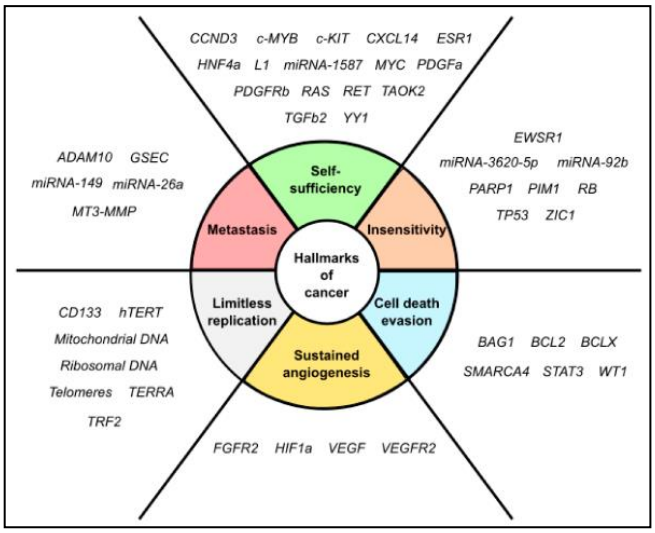

Figure 2.4. Genes containing G-quadruplex structures are associated with cancer hallmarks (Sanchez-Martin et al., 2020)

On the other hand, G-quadruplex folding is shown to be elevated in cancer tissues compared to healthy tissues as shown by immunohistochemical studies (Biffi, Tannahill, Miller, Howat, & Balasubramanian, 2014). Also, since G4s contribute to genome instability, they might be the trigger of cancer evolution. In the light of this information, it has been found that G4 structures have role in carcinogenesis and malignant phenotype of cancer.

2.4. G-quadruplexes as Drug Targets in Cancer

Although many treatment strategies for cancer are in use and continue to be developed, millions of people suffer from cancer and even die from it every year. At this point, targeted methods have revolutionized the anti-cancer therapies. Among them G4 targeting is an alternative approach, since they are related to genomic instability and regulation. Ligands for these structures can be potential cancer therapeutics acting through stabilization or induction of these structures. Suppressing or inhibiting oncogene expression is found as an effective way for cancer treatments in the last decade. Formation or stabilization of G4 structures has been discussed as a potential therapeutic tool against cancer cells. For this reason, the investigations are focused on three main strategies which have been developed to date as shown in Figure 2.5; telomerase maintenance, reduction of oncogene expression and genome instability (Figueiredo et al., 2024; Palma, Carvalho, Cruz, & Paulo, 2021).

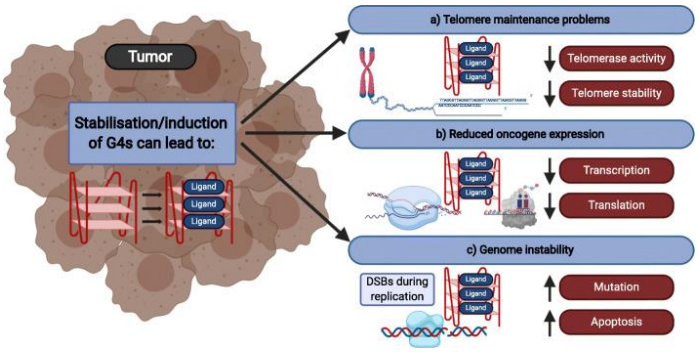

Figure 2.5. The effects of G4 ligands in cancer cells (Palma et al., 2021)

2.4.1. Use of G4 ligand to target telomeres

Human telomeric DNA is around 5-10 kb in which tandem repeats of the motif d[TTAGGG] with a single-stranded 3' of 30–600 long bases are found in double helix DNA sequence (Wojtyla, Gladych, & Rubis, 2011). In each cell division, the end portion of duplex structure is decreased due to end-replication effect, and it is related to cell senescence. To inhibit telomere shortening, telomerase enzyme activity with reverse transcriptase activity is necessary. Telomerase reduce telomere shortening by adding tandem repeats at the end of 3' site. Therefore, this enzyme activity is highly upregulated in cancer cells in which around 85-90% of cancer cells show increase in telomerase expression. During proliferation of cancer cells, telomerase enzyme activity is increased to induce tumour progression and make cancer cells immortal which is related to limitless replication that is one of the hallmarks of cancer (Shay & Wright, 2019). Therefore, development of G4 stabilizer to target G4 structures in the G-rich telomeres can prevent activity of telomerase enzymes and it can be potential therapeutic anti-cancer strategy (Palma et al., 2021).

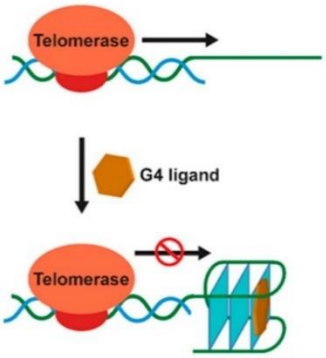

Figure 2.6. The illustration of indirect telomerase inhibition by G4 ligand (Palma et. al. 2021)

2.4.2. Reduced oncogene expression by G4 ligands

Most of oncogene promoters have more G4 structures than promoters of regulatory or tumour suppressor genes (Balasubramanian, Hurley, & Neidle, 2011). It has been found that change in G4 structure can cause decrease in significant oncogene expression level such as VEGF, HIF-1, MYC, BCL-2, KRAS, KIT etc. (Kosiol, Juranek, Brossart, Heine, & Paeschke, 2021). These genes have essential roles in cellular metabolic regulation such as growth, cell survival, cell proliferation, differentiation and cellular signalling and their core of promoter regions are rich in G contents. Therefore, G4 formation in those regions is considered as have effect on transcription level of those genes. Because of these reasons, numerous ligands were developed with the ability to regulate gene expression at G4 level.

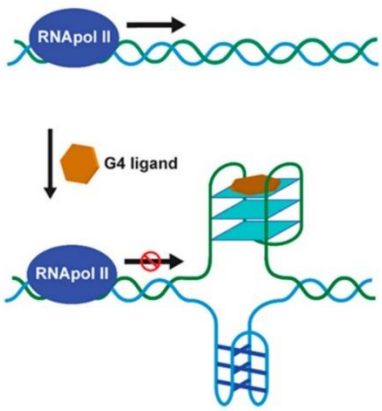

Figure 2.7. The regulation of oncogenes by G4 ligand at transcription level (Palma et al., 2021)

2.4.3. G4 structures and genomic instability

Under specific conditions G4 structures may cause genomic instability. Genomic instability is related to control of G4 formation and unwinding by helicase enzyme activity. Helicases are kind of molecular motors which can act as separating double helix structures of nucleic acids and is highly related to aging and cancer. This enzyme has regulatory roles in cellular metabolism such as DNA replication, repair, recombination, transcription, and telomere maintenance (Mendoza, Bourdoncle, Boulé, Brosh Jr, & Mergny, 2016). G4s can trigger DNA damage which results in genomic instability and apoptosis as well. Therefore, helicase enzyme can be also a target for drug development (Palma et al., 2021).

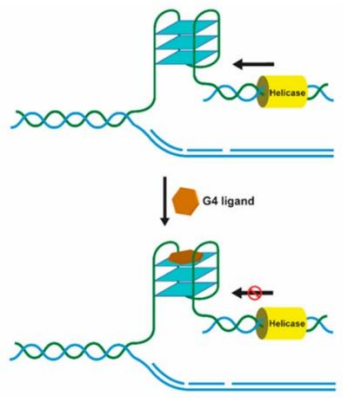

Figure 2.8. The inhibition of helicase activity based on G4 ligand binding (Palma et al., 2021).

2.5. G-quadruplex Ligands

There are various G4 ligands in the literature studies (De Cian et al., 2007). The different molecular features of the distinct G4s enable structure-selective recognition by small molecules (Neidle, 2017). Most of these ligands have common properties such as aromatic core, which provides π–π stacking interactions with flat G4 structures, and positive charges that may interact with DNA or RNA negatively charged backbone phosphate groups in grooves and loops (figure 2.9). Moreover, molecules should be water soluble which can be enabled by protonation of side groups (e.g. amines) around the aromatic ring(s). By this way, the molecule will have both hydrophilic and hydrophobic character at the same time. However, some of them are not suitable as drug when Lipinski's rule of 5 are considered or they do not have suitable ADMET (Absorption-Distribution-Metabolism-Excretion-Toxicity) profiles (Alessandrini, Recagni, Zaffaroni, & Folini, 2021).

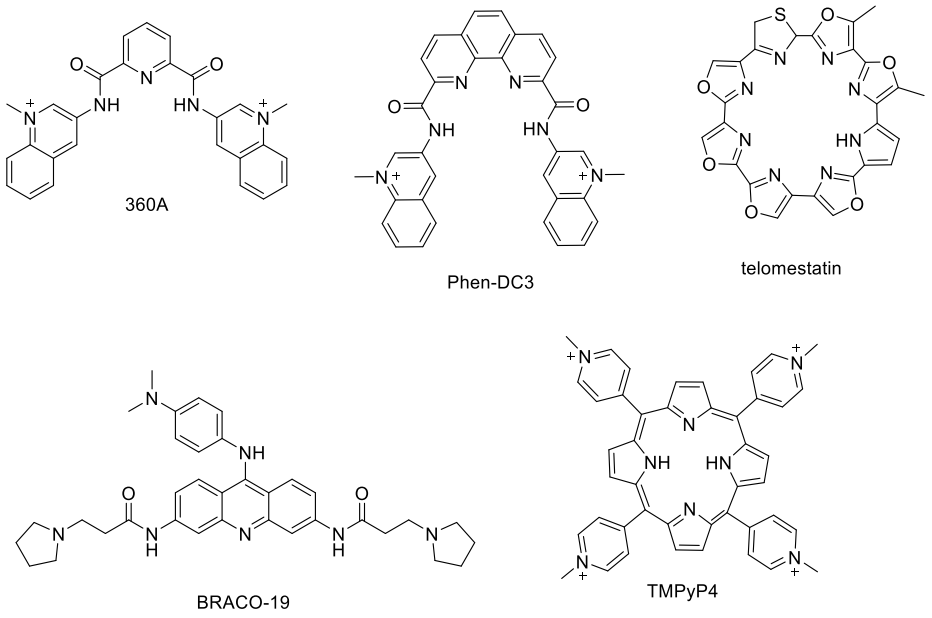

Figure 2.9. Various common G4 ligands in the literature(De Cian et al., 2007)

2.6. G-quadruplex Ligands in Anti-Cancer Therapies as Regulators

There are many designed G4 ligands to downregulate the expression of oncogenes (N. Banerjee, S. Panda, & S. Chatterjee, 2022). For example, FP3 is able to selectively binds to *BCL-2* G4 which is a central protein maintaining a balance between apoptosis and survival. The most known ligand is BRACO-19 which was developed against telomere G4 to inhibit telomerase. IZCZ-3 can selectively bind to *C-MYC* oncogene to inhibit cell progression by cell cycle arrest. Ligand 12459 is a potent G4 stabilizer present in *H-TERT* intron 6. In around 85-90% of all cancer cells telomerase activity is upregulated, which allows the cell to replicate without telomere shortening. G4 structures at telomeres alter telomerase binding and inhibit telomerase activity. This ligand downregulates the expression of telomerase by altering the *H-TERT* splicing pattern, so it also downregulates telomerase activity leading to induction of telomere shortening (Banerjee et al., 2022).

Among these ligands CX-3543 and CX-5461 are in clinical trials. CX-5461 is tried for patients with BRCA-deficient tumours due to its synthetic lethality cause in cancer cells. The other ligand CX-3543, also called as quarfloxin, has passed Phase II trials as a candidate therapeutic agent against several tumours, but Phase III trials were not completed due to its high binding to albumin (Sanchez-Martin et al., 2020).

2.7. Theranostic Agents

Theranostic agent is combination of therapeutic (thera-) and diagnostic (-nostic) agents which has bifunctional/multifunctional capabilities. By using a combine system of diagnosis, treatment, and continuous follow up of a disorder gives advantage. It is considered a diagnostic methodology for personalized therapeutic interventions (Nicolson & Kircher, 2021). A theranostic agent can monitor the disease biomarker or self-report the activity of the agent.

2.8. G-quadruplex Ligands with Theranostic Properties

In recent years, numerous fluorescent probes have been developed for targeting biomolecules such as proteins or nucleic acid structures. However, these molecules also have the disadvantages of having high toxicity and low membrane permeability. Therefore, novel near-infrared (NIR) or far-red probes have been designed which have less off-target effects (Shinziya, Menon, & Das, 2024). These molecules have share some common structures or functional groups like flat aromatic rings on the structure for stacking between G4 planes, donor atoms for hydrogen bonding with DNA, cationic charge interacting groups with DNA negatively charged phosphates etc. Moreover, some of these probes have been designed as multifunctional such as therapeutic while being diagnostic. There are many synthesized structures in the literature as theranostic agent which can be sensitive to light or pH change (activatable) or emission change upon binding to nucleic acids and biomolecules. Naphthalene, thiazole and cyanine derivatives are frequently used for this purpose in both in vitro and in vivo studies. As an example of these probes, Liu *et al.* developed thiazole-based styryl derivatives as fluorescent NIR probe which has high selectivity for G4 DNA and exhibited biological activities similar to those of theranostic agents (L. Zhang et al., 2020). There are also activatable fluorescent probes like Guan *et al.* designed a benzothiophenyl rotor which is an activatable cyanine probe. In this study, about 98-fold enhanced fluorescence was observed when this molecule was interacted with G4 regions of *C-MYC* genes (Guan et al., 2023).

In another study reported by Suseela and Govindaraju *et al.* a neocuproine-based derivatives named TGP18 was synthesized as G4 theranostic agent that could display high selectivity for G4 structures in promoter region of *BCL-2* gene resulting in

fluorescence increase. Since *BCL-2* is an anti-apoptotic gene, when TGP18 ligand suppressed *BCL-2* gene expression at transcription level, genome instability was triggered leading to DNA damage and apoptosis. In vivo studies was also conducted with lung cancer mice models (Suseela, Satha, Murugan, & Govindaraju, 2020).

BODIPY (boron-dipyrromethene) is also one of the fluorescent dyes which has emission in visible spectrum (the main body) mostly used in fluorescent imaging techniques. They can be modified by adding functional groups to shift the emission wavelength from visible spectrum to NIR or far-red spectra. Therefore, BODIPY derivatives are highly preferred in cell imaging studies in biology as well. Moreover, BODIPY has advantages such as high fluorescence quantum yield, low toxicity, low polarity, low photodegradation and biocompatibility and become easily manipulated (Ahmad et al., 2025; Kumar, Saxena, & Joshi, 2025). It is known that BODIPY main body can easily intercalate G-quadruplex structures via π-π stacking interactions (P. L. Zhang, Wang, Chen, Du, & Gao, 2019). Therefore, BODIPY derivatives are commonly used as G-quadruplex ligands for therapeutic and/or diagnostic purposes as well (Baser et al., 2023). Distyryl pyridinium BODIPYs were used as G4 stabilizers by Erbas-Cakmak research group and they are shown to downregulate oncogene expression (Uyar et. al. 2023; Baser et. al. 2023).

3. MATERIALS AND METHODS

Within the scope of the study two different molecules were designed as G4 ligands; one of them is expected to bind to G4 structures of nucleic acids, and through stabilization and/or DNA alkylation (L1), the other one is a theranostic agent which displays a fluorescence output beside G4 stabilization (L2). There is one control ligand L3 with monostyryl pyridinium structure lacking any fluorescent or alkylating agent on the structure. L1 is the chlorambucil attached derivative of GQ1 (molecule 5, Scheme 3.1) developed by our group (Baser et al., 2023). GQ1 has found to influence adaptation of cellular metabolism of cancer cells to their microenvironment by inducing downregulation of oncogenes related to metabolic pathway such as GLUT1, HIF1-α, PDK1, and COX4-II which have G4 structures at their promoter or proximal sites. Therefore, L1 was designed based on this knowledge and proof to understand its effect on cellular metabolism in this project as well. Firstly, all molecules were synthesized and purified. Purification techniques include extraction, column chromatography and precipitation. The structural characterization of molecules was performed by ^{1}H, ^{13}C Nuclear Magnetic Resonance (NMR) Spectroscopy and/or High-Resolution Mass Spectrometry (QTOF-LC/MS). G4 binding of the ligand molecules were tested using FRET Melting assay. MTT cell viability assay was performed on human breast cancer cells (MCF-7 cell line). The gene expression analysis was performed by RNA extraction, cDNA synthesis and by using RT-PCR. Also, theranostic capacity of the ligand L2 was tested by tracking emission change of the molecules upon increase in oligomer concentration. DNA alkylation of L1 was analysed by urea-PAGE gel electrophoresis method.

3.1. Design, Synthesis and Characterization of Compounds

3.1.1. Design of ligand L1

The compound L1 has anticancer agent chlorambucil (red) on its structure which causes genomic instability through DNA alkylation on guanines (Figure 3.1). Pyridinium distyryl BODIPY core structure is chosen as G-quadruplex ligand, since previously, highly strong and selective binding to G4 motifs is reported to regulate oncogene expression and reprogram cancer cell metabolism in MCF7 cells (Baser et. al. 2023). By

binding these two anti-cancer agents, therapeutic potential of the ligand is aimed to be enhanced.

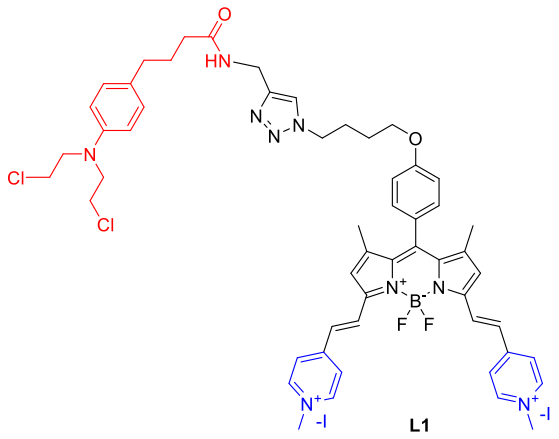

Figure 3.1. The structure of the G4 ligand L1

This chlorambucil unit (red part) was assembled with cationic compound **5** by Huisgen 1,3-cycloaddition reaction in the last step (Scheme 3.1). The binding of chlorambucil to the propargyl unit via an amide bond and functionalization via cycloaddition reaction with high efficiency has been reported in the literature (Di Antonio, McLuckie, & Balasubramanian, 2014). In the first step, compound 1 was obtained by bromination of 4-hydroxybenzaldehyde with 1,3-dibromobutane in the presence of K_2CO_3. The next step (**2**) was obtained from the reaction between compound 1 and sodium azide to attach azide unit to the upward end of the molecule. Then, the general BODIPY synthesis was done by attaching compound 2. This molecule was functionalized by using Knoevenagel condensation reaction with 4-pyridinecarboxaldehyde in the presence of piperidine and acetic acid in the solvent of benzene. Dean-Stark apparatus was used at this step to remove the resulting water and improve the yield. Next, the molecule 5 was methylated to obtain cationic pyridinium derivatives (blue parts). In the previous study, compound 5 was successfully synthesized and tested in mitochondrial metabolism pathway in vitro (Baser et al., 2023). The last step was attachment of chlorambucil through Cu(I)-catalysed azide-alkyne cycloaddition reaction to obtain the target ligand L1. The details of each step and the characterization information was given below.

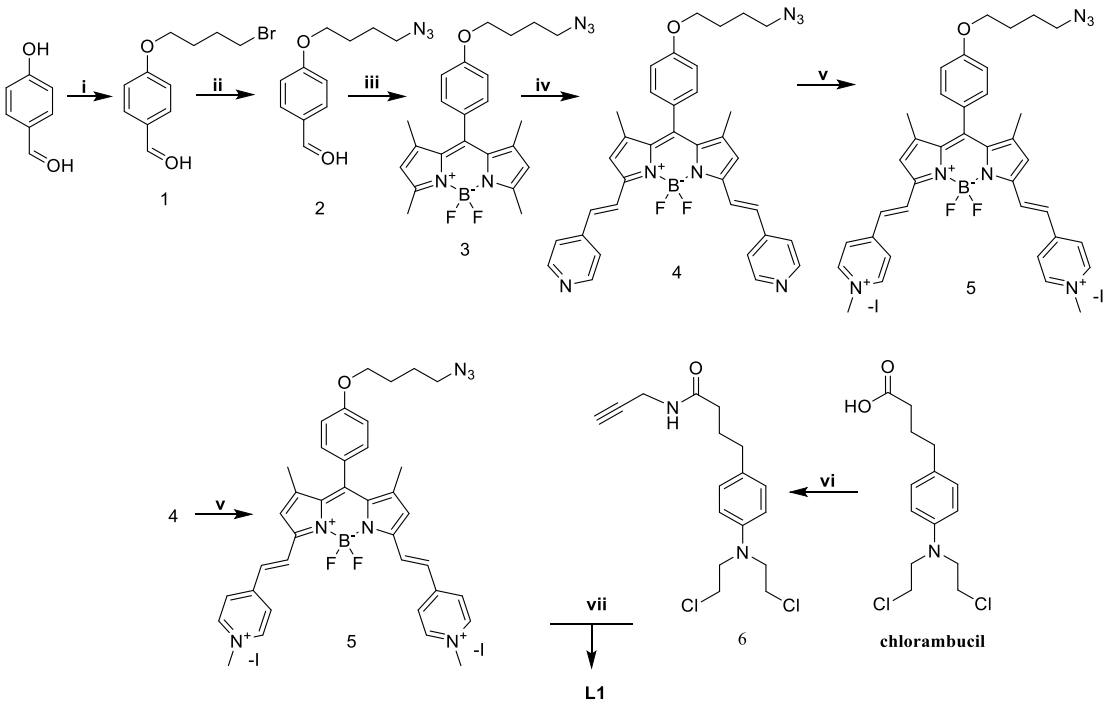

Scheme 3.1. The synthesis scheme of compound L1. Reaction conditions: i) 1,4-dibromobutane, K_2CO_3, DMF ii) NaN_3, DMSO, 60°C iii.a) 2,4-dimethylpyrrole, TFA, DCM, N_2 iii.b) p-chloranil iii.c) Et_3N, $BF_3.OEt_2$ iv) 4-pyridinecarboxaldehyde, acetic acid, piperidine, benzene, 90°C v) CH_3I, DMF vi) propargylamine, DMAP, DCC, DCM vii) $Cu(I)MeCN_4PF_6$, DCM.

3.1.2. Synthesis of compound 1

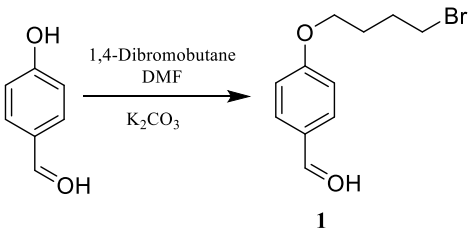

Scheme 3.2. Synthesis scheme of compound 1

The compound was synthesized using the literature procedure (Baser et. al. 2023). 2.44 grams of 4-hydroxybenzaldehyde (20 mmol) was dissolved in 20 mL of dimethyl formamide. 5.5 grams of K_2CO_3 (36 mmol, 1.8 eq.) and 4.8 mL of dibromobutane (40 mmol, 2 eq.) were added to the solution and stirred for 18h at room temperature. After the solid part was removed by filtration, the solvent was removed by vacuum evaporator. The product mixture was extracted with water and dichloromethane (DCM). The organic phase was collected and dried with Na_2SO_4, then the solvent was removed under reduced pressure by vacuum evaporator. It was purified by silica gel column chromatography

using hexane: ethyl acetate mobile phase mixture (4:1; v/v) and a white solid pure product was obtained as 3.76 g with 73% yield.

^{1}H NMR (400 MHz, $CDCl_3$): δ ppm; 9.86 (s, 1H), 7.81 (d, 2H, J = 8.9 Hz), 6.97 (d, 2H, J = 8.7 Hz), 4.06 (t, 2H, J = 6.0 Hz), 3.47 (t, 2H, J = 6.5 Hz), 2.10-1.90 (m, 4H).
^{13}C NMR (101 MHz, $CDCl_3$): δ ppm; 191.11, 164.15, 132.21, 130.27, 114.99, 67.59, 33.46, 29.53, 27.92.

3.1.3. Synthesis of compound 2

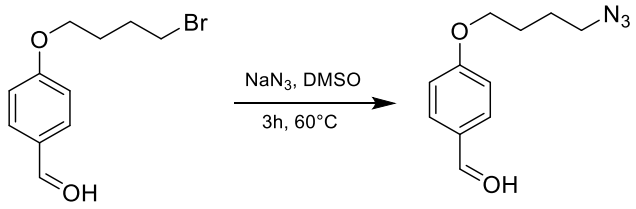

1 **2**

Scheme 3.3. Synthesis scheme of compound 2

The compound was synthesized using the literature procedure (Baser et. al. 2023). 2.57 grams of compound **1** (10 mmol) was dissolved in 15 ml of dimethyl sulfoxide (DMSO). Then, 975 mg of sodium azide (NaN_3) (15 mmol, 1.5 eq.) were added and stirred for 3 hours at 60°C. After the reaction was cooled to room temperature, extraction was performed with diethyl ether and water. The ether phase was extracted with water 3 more times to remove DMSO. The organic phase was collected and dried with Na_2SO_4, then the solvent was removed under vacuum. The conversion was followed based on the shift of the proton adjacent to bromine in the ^{1}H NMR spectrum, and it was determined that all of the starting material was converted to product. The reaction was carried out with quantitative yield and proceeded to the next step without the need for additional purification.

^{1}H NMR (400 MHz, $CDCl_3$): δ ppm; 9.84 (s, 1H), 7.79 (d, 2H, J=8.8 Hz), 6.96 (d, 2H, J=8.7 Hz), 4.04 (t, 2H, J=6.1 Hz), 3.42 (t, 2H, J=6.7 Hz), 1.87 (m, 2H), 1.79 (m, 2H).
^{13}C NMR (101 MHz, $CDCl_3$): δ ppm; 191.109, 164.18, 132.18, 130.39, 114.84, 67.81, 51.30, 26.54, 25.85.

3.1.4. Synthesis of compound 3

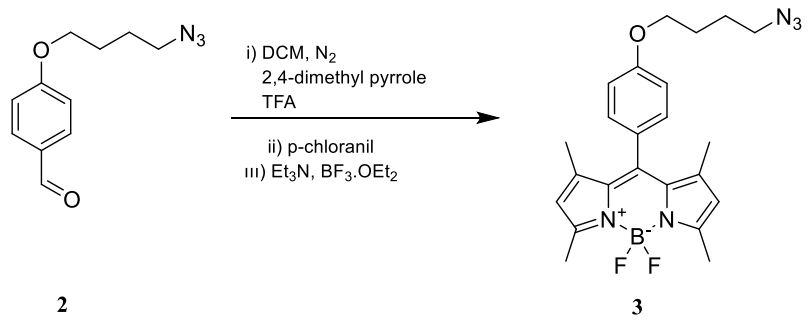

2 3

Scheme 3.4. Synthesis scheme of compound 3

The compound was synthesized using the literature procedure (Baser et. al. 2023). 2.0 grams of compound **2** (9.13 mmol) was dissolved in 125 ml of DCM and kept under N_2 gas for 20 min. Then, 2.35 mL of 2,4-dimethylpyrrole (22.83 mmol, 2.5 eq.) and catalytic amount (5 drops) of trifluoroacetic acid were added and stirred for 18h at room temperature under nitrogen gas. After, 1.7 g of p-chloranil was added and stirred for 2.5 h at room temperature. 7 mL of triethylamine and 7 mL of boron trifluoride diethyl etherate were added successively and stirred for 2.5 h at room temperature. Extraction was done with water and dichloromethane. The organic phase was collected and dried with Na_2SO_4, then the solvent was removed under reduced pressure by vacuum evaporator. It was purified by silica gel column chromatography using DCM: hexane (5:3; v/v) as mobile phase. 500 mg of orange solid product was obtained with 13% yield.

^{1}H NMR (400 MHz, $CDCl_3$) δ 7.04 (d, J = 8.6 Hz, 2H), 6.97 (d, J = 8.6 Hz, 2H), 5.96 (s, 2H), 4.02 (t, J = 5.9 Hz 2H), 3.37 (t, J = 6.6 Hz, 2H), 2.53 (s, 6H), 1.97 – 1.70 (m, 4H), 1.42 (s, 2H).

3.1.5. Synthesis of compound 4

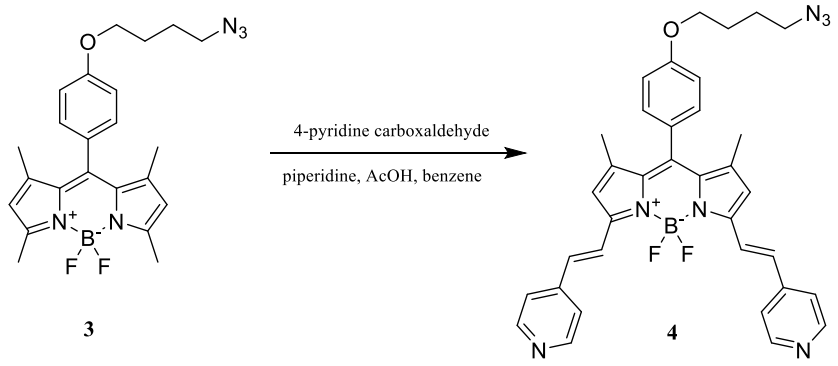

Scheme 3.5. Synthesis scheme of compound 4

The compound was synthesized using the literature procedure (Baser et. al. 2023). 0.28 grams of compound **3** (0.64 mmol) was dissolved in 20 mL of benzene. Then, 238 µL of 4-pyridine carboxaldehyde (2.51 mmol, 3.92 eq.), 460 µL of piperidine 460 µL of acetic acid were added to the solution. Reflux was performed with a Dean-Stark apparatus at 90°C, slightly above the boiling point of benzene. With this reflux, benzene and water formed as a reaction byproduct were removed from the reaction flask and collected. By this way, Knoevenagel condensation was performed and compound **4** was obtained. Extraction was done with water and DCM. The organic phase was collected and dried with Na_2SO_4, then the solvent was removed under reduced pressure by vacuum evaporator. The substance was purified by silica gel column chromatography using DCM: hexane (2:1; v/v) mobile phase. A solid blue-purple product was obtained with a yield of 13%.

^{1}H NMR (400 MHz, Chloroform-d) δ 8.57 (d, J = 6.1 Hz, 4H), 7.82 (d, J = 16.3 Hz, 2H), 7.40 (d, J = 6.3 Hz, 4H), 7.14 (d, J = 8.6 Hz, 2H), 7.08 (d, J = 16.3 Hz, 2H), 6.97 (d, J = 8.7 Hz, 2H), 6.61 (s, 2H), 4.00 (t, J = 6.0 Hz, 2H), 3.34 (t, J = 6.6 Hz, 2H), 1.95 – 1.83 (m, 2H), 1.83 – 1.71 (m, 2H), 1.46 (s, 6H).

3.1.6. Synthesis of compound 5

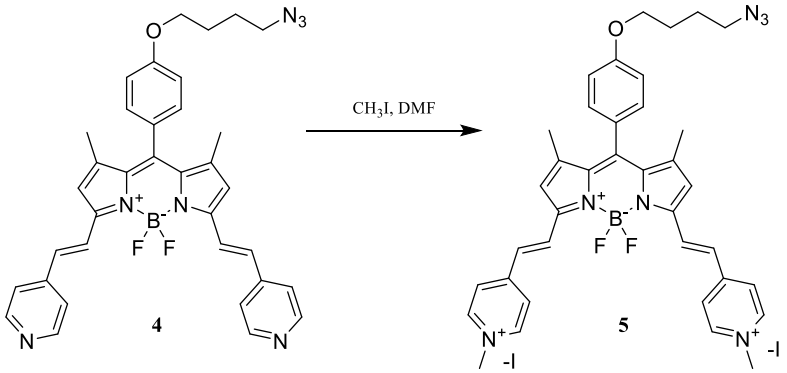

Scheme 3.6. Synthesis scheme of compound 5

The compound was synthesized using the literature procedure (Baser et. al. 2023). 0.0491 grams of compound **4** (0.079 mmol) was dissolved in 3 ml of dimethylformamide (DMF) and 500 µL of iodomethane was added. It was left to stir at room temperature for 2 days. At the end of 2 days, the reaction was checked by TLC with 10% methanol-DCM system. When it was understood that the compound **4** was consumed and the green compound **5** was formed, the reaction was terminated. The solvent DMF was removed in a rotary evaporator and the product was precipitated in ethyl acetate. The precipitated product was washed with ethyl acetate and dark green compound **5** was obtained in 100% yield.

^{1}H NMR (400 MHz, DMSO-d 6) δ 8.90 (d, J = 6.6 Hz, 4H), 8.20 (d, J = 7.1 Hz, 4H), 7.94 (d, J = 16.2 Hz, 2H), 7.83 (d, J = 16.3 Hz, 2H), 7.39 (d, J = 8.6 Hz, 2H), 7.25 – 7.05 (m, 3H), 4.32 (s, 6H), 4.11 (t, J = 6.3 Hz, 2H), 3.44 (t, J = 6.7 Hz, 2H), 1.83 (q, J = 6.7, 6.1 Hz, 2H), 1.79 – 1.68 (m, 2H), 1.55 (s, 6H).

3.1.7. Synthesis of compound 6

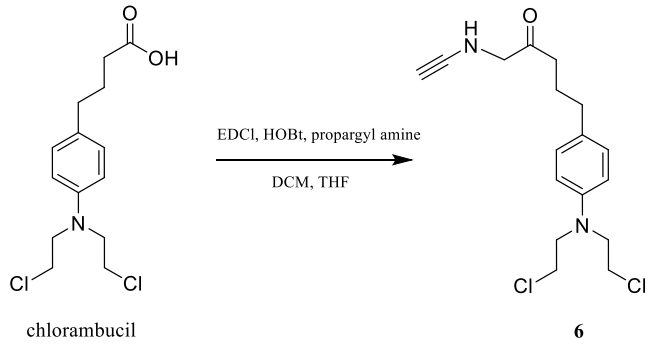

Scheme 3.7. Synthesis scheme of compound 6

305 mg of chlorambucil (1 mmol) was dissolved in 8 mL of DCM and 2 mL of tetrahydrofuran (THF). 234 mg of EDCl (1-ethyl-3-(3-dimethyl amino propyl)-3-ethylcarbodimide hydrochloride), 204 mg of HOBt (1-hydroxybenzotriazole hydrate) were added. 128 ml of propargylamine (2 mmol, 2 eq.) were added. The reaction was closed and left to stir overnight at room temperature. It was purified by silica column chromatography using 5% methanol in dichloromethane as mobile phase. Thus, a light-yellow solid product was obtained as 273 mg with 80% yield.

^{1}H NMR (400 MHz, $CDCl_3$) δ 7.00 (d, J = 8.7 Hz, 2H), 6.55 (d, J = 8.7 Hz, 2H), 5.48 (b, 1H), 3.97 (dd, J = 5.2, 2.6 Hz, 2H), 3.69 – 3.60 (m, 4H), 3.60 – 3.45 (m, 4H), 2.50 (t, J = 7.4 Hz, 2H), 2.16 (t, J = 2.6 Hz, 1H), 2.14 – 2.04 (m, 2H), 1.94 – 1.79 (m, 2H).
^{13}C NMR (101 MHz, $CDCl_3$) δ 172.38, 144.38, 130.50, 129.72, 112.20, 79.59, 71.63, 53.62, 40.53, 35.54, 33.95, 29.18, 27.11.
HRMS: Teoritical m/z $(M+H)^+$: 341.1187, Experimental m/z (M+H) + : 341.11827, Δ=1.26 ppm

3.1.8. Synthesis of compound L1

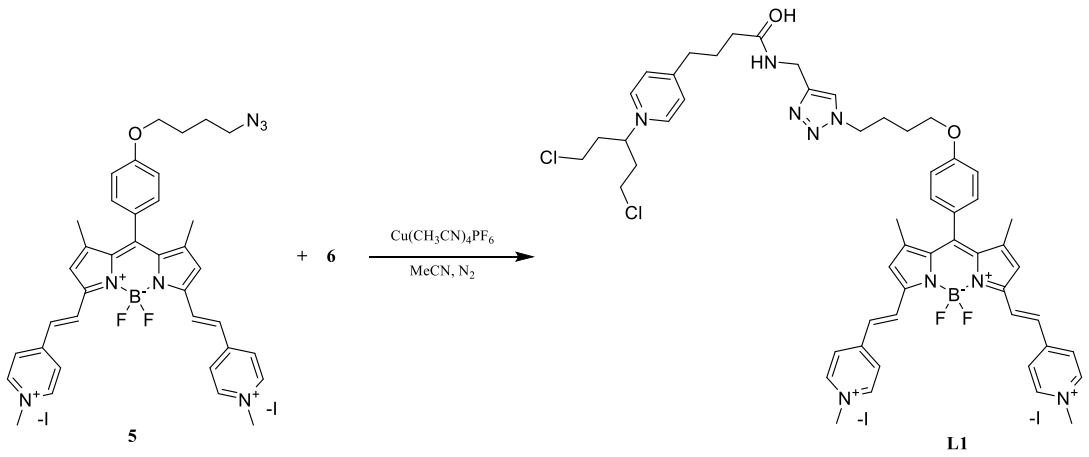

Scheme 3.8. Synthesis scheme of compound L1

65 mg of compound **5** (72 mmol) and 90 mg of compound **6** (262 mmol) were dissolved in 10 mL of acetonitrile (MeCN) in the presence of 102 mg of tetrakis copper (I) hexofluorophosphate ([Cu $(CH_3CN)_4]PF_6$). The flask was capped, and a nitrogen balloon was placed on it. It was left to stir at room temperature for 24 hours. The amount of acetonitrile was reduced by the rotary evaporator, and ethyl acetate was added to precipitate the product. As a result of the reaction, a dark green solid product was obtained as 15 mg with a yield of 23%.

^{1}H NMR (400 MHz, DMSO-d_6) δ 8.90 (d, J = 6.6 Hz, 4H), 8.30 (t, J = 5.6 Hz, 1H), 8.19 (d, J = 6.8 Hz, 4H), 7.99 –7.91 (m, 3H), 7.82 (d, J = 16.3 Hz, 2H), 7.37 (d, J = 8.6 Hz, 2H), 7.18 (s, 2H), 7.15 (d, J = 8.5 Hz, 2H), 7.00 (d, J = 8.6 Hz, 2H), 6.65 (d, J = 8.7 Hz, 2H), 4.43 (t, J = 7.0 Hz, 2H), 4.31 (m, 8H), 4.07 (t, J = 6.4 Hz, 2H), 3.69 (d, J = 4.7 Hz, 8H), 2.45 (m, 2H), 2.16 (m, 2H), 1.99 (t, J = 7.5 Hz, 2H), 1.73 (m, 4H), 1.54 (s, 6H).

^{13}C NMR (101 MHz, DMSO-d_6) δ 172.41, 160.09, 151.17, 150.84, 146.10, 144.86, 135.75, 132.07, 130.40, 129.77, 127.69, 124.75, 123.40, 121.34, 115.87, 112.34, 67.57, 52.67, 49.43, 47.81, 41.62, 35.20, 34.64, 34.07, 27.79, 27.06, 26.10, 15.11.

HRMS: Teoritical m/z (M) 2^+ : 492.7154, Experimental m/z (M) $^{2+}$: 492.71577, Δ=0.75 ppm

3.1.9. Design of ligand L2

The compound L2 has two different modules having pyridinium BODIPY-based structure used with the intention of G4 stabilisation and an anthracene moiety which is expected to display fluorescence as the triazolium unit on the structure is shielded upon G4 interaction. Triazolium unit in the vicinity is known to quench the fluorescence of anthracene (blue, Figure 3.9) through photoinduced electron transfer. When the energy level is destabilized through G4 interaction, electron transfer is expected to be blocked. Mono-styryl pyridinium unit is attached to the meso position of the BODIPY (red module) to benefit from positive charges and stacking interactions.

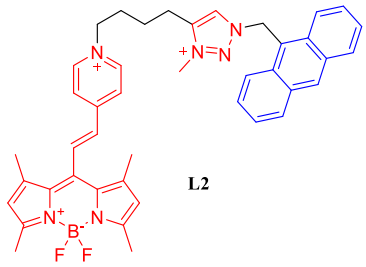

Figure 3.2. The structure of novel theranostic G4 ligand L2

Firstly, BODIPY-based site and anthracene module were synthesized separately. When BODIPY module was obtained, it was allowed to assemble with anthracene unit by copper (I) catalyzed click reaction. Modules were prepared starting with synthesis of BODIPY (8) from acetyl chloride and 2,4-dimethyl pyrrole. Then, this molecule was reacted with pyridine carboxaldehyde through Knoevenagel condensation reaction in the presence of piperidine and acetic acid in the solvent of benzene, and compound 9 was obtained. The compound 10 (L3) was formed by quaternization of pyridine with 6-iodo-1-hexyne to incorporate an alkyne unit necessary for the next click reaction. The compound 11 was obtained from the reaction of sodium azide with 9-chloromethylanthracene. Firstly, compound 10 (L3) was dissolved in DCM and compound 11 was added to reaction in the presence of tetrakis(acetonitrile)copper(I) hexafluorophosphate for click reaction (12). Lastly, triazole on the compound 12 was methylated with the use of methyl iodide (L2).

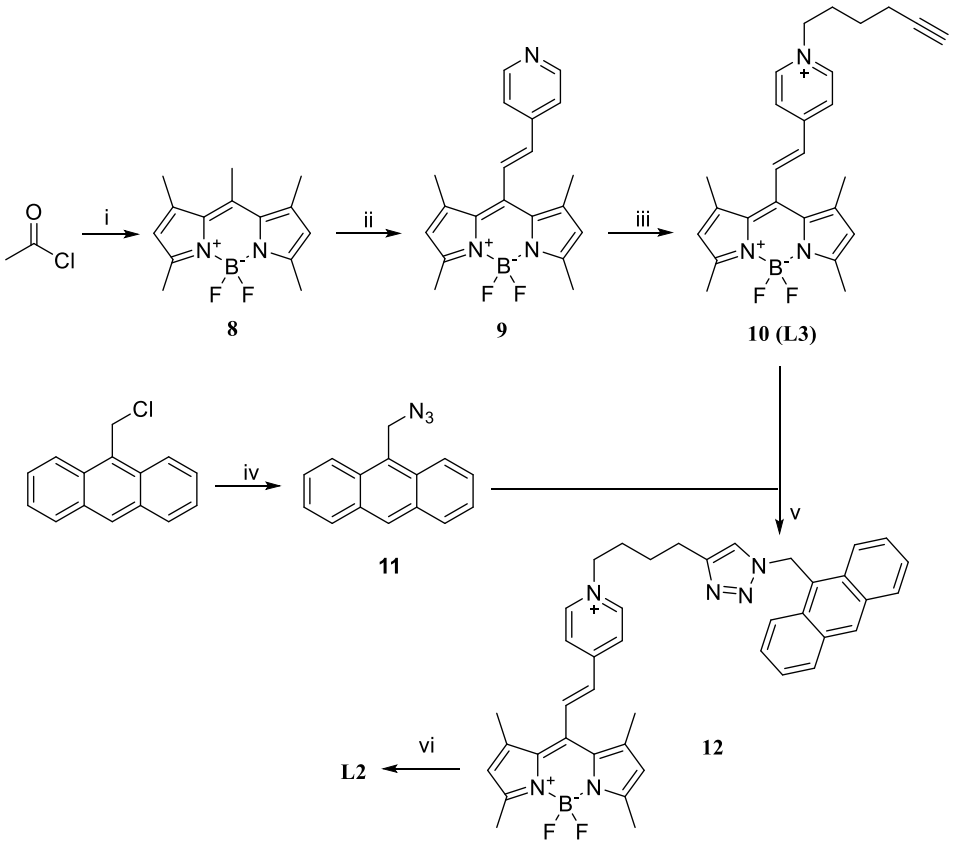

Scheme 3.9. The synthesis scheme of compound L2. Reaction conditions: i) Et_3N, BF_3OEt_2, DCM, N_2 (ii) 4-pyridine carboxaldehyde, benzene, AcOH, piperidine, 90°C, reflux, 3h (iii) DCM, DMF, 1-iodo-6-hexyne, 50°C (iv) NaN_3, DMSO, 60°C, 3h v) Cu(I)$MeCN_4PF_6$, DCM, MeCN vi) MetI, DMF.

3.1.10. Synthesis of compound 8

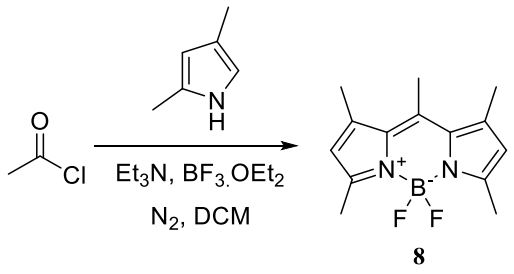

Scheme 3.10. Synthesis scheme of compound 8

2 mL of 2,4-dimethylpyrrole and 30 mL of DCM were placed in a round-bottom flask and kept under N_2 gas for 10 minutes. Then 700 µL of acetyl chloride was added and kept under N_2 gas for 8 minutes. The reaction was left to mix overnight. The next day, 8 mL of $BF_3.OEt_2$ (Boron trifluoride diethyl etherate complex) and 6 mL of

triethylamine were added to the reaction mixture which was then stirred for 4 hours at room temperature. The reaction was followed periodically by thin layer chromatography (TLC) hexane: ethyl acetate system (3:1; v/v). Extraction was done with DCM-water after 4 hours. The organic phase was collected and dried over Na_2SO_4, then filtered through filter paper and transferred to a round-bottom flask. The solvent was removed under reduced pressure. The obtained substance was purified using silica gel column chromatography with a gradually changing mobile phase system from hexane: ethyl acetate (500:1; v/v) to hexane: ethyl acetate (2:1; v/v). The pure product was obtained as 564 mg with 22% yield as orange powder-like substance.

^{1}H NMR (400 MHz, Chloroform-d) δ 5.98 (s, 2H), 2.51 (s, 3H), 2.45 (s, 6H), 2.34 (s, 6H).
^{13}C NMR (101 MHz, $CDCl_3$) δ 153.62, 141.41, 140.99, 132.07, 121.25, 17.33, 16.39, 14.43.
HRMS: Theoritical value for $(M+H)^+$: 263.15256, Experimental Value for $(M+H)^+$: 263.15239, Δ=0.65 ppm.

3.1.11. Synthesis of compound 9

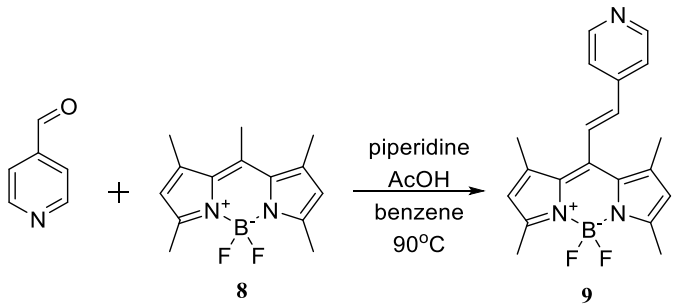

8 **9**

Scheme 3.11. Synthesis scheme of compound 9

214 mg of compound **8** (0.8 mmol) was dissolved in 10 mL of benzene. 128 µL of 4-pyridinecarboxaldehyde (1.2 mmol, 1.5 eq.), 0.5 mL acetic acid and 0.4 mL piperidine were added into mixture and refluxed at 90°C. The reaction was followed by TLC with MetOH : EtoAc (1:19; v/v) solvent system. When the product was formed, the mixture was extracted with DCM-water and dried over Na_2SO_4. The solvent was removed

under reduced pressure with vacuum evaporator. The substance was purified by silica gel column chromatography with MetOH : EtoAc (1:19; v/v) mobile phase system. The pure product was obtained as 114 mg with 40% yield as dark orange powder-like substance.

^{1}H NMR (400 MHz, Chloroform-d) δ 8.60 (d, J = 6.1 Hz, 2H), 7.29 (d, J = 6.2 Hz, 2H), 7.23 (1H, part of the peak is under the chloroform peak), 6.65 (d, J = 16.4 Hz, 1H), 6.00 (s, 2H), 2.48 (s, 6H), 2.11 (s, 6H).
^{13}C NMR (101 MHz, $CDCl_3$) δ 155.69, 150.74, 142.83, 141.83, 138.29, 135.47, 130.92, 126.70, 121.41, 120.80, 16.99, 14.66.
HRMS: Theoritical value for $(M+H)^+$: 352.17911, Experimental Value for $(M+H)^+$: 353.17884, Δ=0.77 ppm.

3.1.12. Synthesis of compound 10 (L3)

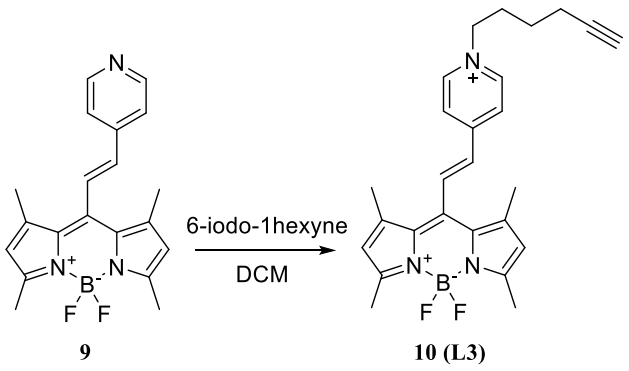

Scheme 3.12. Synthesis scheme of compound 10

114 mg compound **9** (0.32 mmol) was dissolved in 3.2 mL of DMF and 75 µL 6-iodohexyne was added. The reaction was left at 50°C for 3 days and followed by TLC until the product was formed. Then, the solvent was removed by rotary evaporator. The reaction mixture was extracted with DCM-water and organic phase was dried with Na_2SO_4 to get rid of any water droplets. The solvent was removed under reduced pressure with vacuum evaporator. The substance was purified by silica gel column chromatography with MeOH: DCM (1:9; v/v) mobile phase system. The pure product was obtained as 105 mg as dark violaceus sticky substance with 59% yield.

^{1}H NMR (400 MHz, Chloroform-d) δ 9.23 (d, J = 6.9 Hz, 2H), 8.12 (d, J = 6.8 Hz, 2H), 7.87 (d, J = 16.3 Hz, 1H), 6.82 (d, J = 16.3 Hz, 1H), 6.01 (s, J = 1.0 Hz, 2H), 4.89 (t, J = 7.7 Hz, 2H), 3.67 (s, 3H), 2.47 (s, 6H), 2.26 (td, J = 6.8, 2.7 Hz, 2H), 2.20 – 2.11 (m, 2H), 2.08 (s, 6H), 1.94 (t, J = 2.6 Hz, 1H), 1.70 – 1.58 (m, 2H).
^{13}C NMR (101 MHz, $CDCl_3$) δ 156.83, 151.38, 145.04, 141.73, 136.61, 135.52, 131.65, 130.36, 125.16, 121.92, 82.98, 69.91, 63.73, 61.05, 30.69, 29.71, 24.51, 17.93, 17.24, 14.76.
HRMS: Theoritical value for $(M)^+$: 432.24171, Experimental Value for $(M)^+$: 432.24272, Δ=2.36 ppm.

3.1.13. Synthesis of compound 11

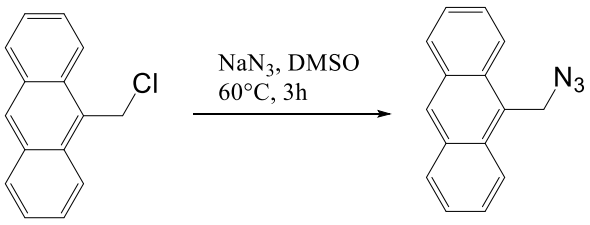

11

Scheme 3.13. Synthesis scheme of compound 11

757 mg of 9-chloromethylanthracene (3.34 mmol) and 325 mg of NaN_3 (5 mmol) were dissolved in 10 mL of DMSO. The mixture was stirred for 3 hours at 60°C. Then, the extraction was done with diethyl ether and water. The organic phase was collected and dried with Na_2SO_4. The solvent was removed by rotary evaporator. No additional purification was required, and 780 mg of pure yellow product was obtained from the reaction with a quantitative yield.

^{1}H NMR (400 MHz, $CDCl_3$) δ 8.53 (s, 1H), 8.31 (d, *J* = 8.9 Hz, 2H), 8.07 (d, *J* = 8.4 Hz, 2H), 7.72 – 7.58 (m, 2H), 7.58 – 7.41 (m, 2H), 5.35 (s, 2H).
^{13}C NMR (100 MHz, $CDCl_3$) δ 131.4, 130.7, 129.3, 129.0, 126.9, 125.8, 125.2, 123.5, 46.4.
HRMS: Theoritical value for $(M\text{-}N_2\text{+}H)^+$: 206.0970, Experimental Value for $(M\text{-}N_2\text{+}H)^+$: 206.09864, Δ=7.96 ppm.

3.1.14. Synthesis of compound 12

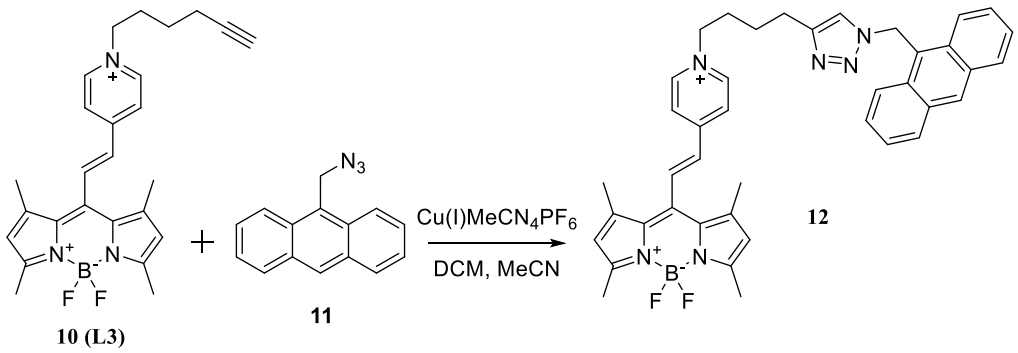

Scheme 3.14. Synthesis scheme of compound 12

52.6 mg of compound **10** (0.09 mmol) was dissolved in 3 mL DCM and 134.2 mg of Tetrakis(acetonitrile)copper(I) hexafluorophosphate (0.35 mmol, 3 eq.) was added. 1 mL of acetonitrile was added to increase the solubility of Cu (I) salt and then 84.6 mg of compound **11** (0.36 mmol, 3 eq.) was added. The mixture was left to be stirred at room temperature for 2 days. The reaction was checked with TLC by different mixtures of MetOH-DCM systems. The reaction mixture was extracted with DCM and water. The organic phase was dried with Na_2SO_4 and the solvent was removed by vacuum evaporator under reduced pressure. It was purified by silica gel column chromatography with first %5 MetOH-DCM (1:20, v/v) and then %10 MetOH-DCM (1:10, v/v) systems.

^{1}H NMR (400 MHz, Chloroform-*d*) δ 8.55 (d, *J* = 6.5 Hz, 2H), 8.44 (s, 1H), 8.31 (d, *J* = 9.0 Hz, 2H), 7.94 (d, *J* = 8.5 Hz, 2H), 7.79 (d, *J* = 6.5 Hz, 2H), 7.59 – 7.46 (m, 2H), 7.46 – 7.35 (m, 2H), 7.12 (s, 1H), 6.63 (d, *J* = 16.3 Hz, 1H), 6.39 (s, 2H), 5.97 (s, 2H), 4.39 (t, *J* = 7.6 Hz, 2H), 2.49 (d, *J* = 14.2 Hz, 8H), 1.98 (m, 8H).
HRMS: Theoritical value for $(M)^+$: 665.33701, Experimental Value for $(M)^+$: 665.33850, Δ=2.24 ppm.

3.1.15. Synthesis of compound L2

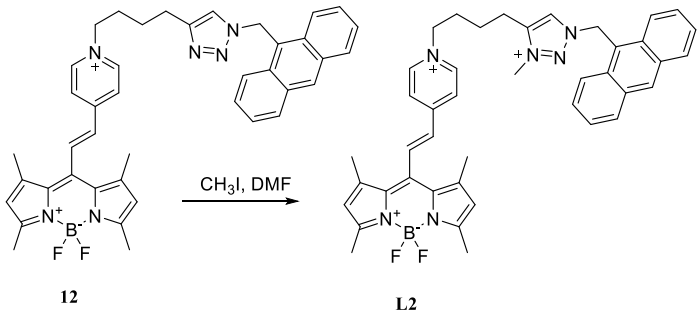

Scheme 3.15. Synthesis scheme of compound L2

60 mg of compound **12** was dissolved in 2 mL of DMF and 400 µL of methyl iodide was added to the mixture and left to be stirred for 2 days at room temperature. When the formation of product was observed, DMF was removed by vacuum evaporator under reduced pressure. The substance was washed with ethyl acetate-hexane (1:3, v/v) solvent mixture to get rid of the remaining DMF. It was purified by silica gel column chromatography with MetOH-DCM (1:9, v/v) mobile phase system. The pure product was obtained with a quantitative yield.

^{1}H NMR (400 MHz, Chloroform-*d*) δ 8.55 (d, *J* = 6.5 Hz, 2H), 8.48 (s, 1H), 8.35 (dd, *J* = 8.9, 1.1 Hz, 2H), 8.11 – 7.92 (m, 2H), 7.79 (d, *J* = 6.4 Hz, 2H), 7.57 (ddd, *J* = 9.0, 6.6, 1.4 Hz, 2H), 7.55 – 7.39 (m, 2H), 7.18 (s, 1H), 6.64 (d, *J* = 16.3 Hz, 1H), 6.42 (s, 2H), 6.01 (s, 2H), 4.42 (t, *J* = 7.6 Hz, 2H), 3.49 (s, 3H), 2.53 (s, 8H), 2.00 (s, 10H).
HRMS: Theoritical value for $(M+HCO_2^-)^+$: 825.35814, Experimental Value for $(M+HCO_2^-)^+$: 825.32844, Δ=35.98 ppm.

3.2. FRET Melting Assay

Within the scope of this project, all designed molecules were expected to bind to G4 regions of DNA. The detection of this kind of binding was performed Förster Resonance Energy Transfer (FRET) melting assay. FRET assay aims to denaturation of DNA secondary structures and their stabilization by using compounds known as DNA binders that some of them have high interaction with G-quadruplex DNAs compared to duplex DNAs. The principle is based on the molecular excitation energy transfer between

donor and acceptor. The donor and acceptor molecules should be at a distance less than approximately 10 nm. In FRET melting assay the target molecule is covalently labeled with donor and acceptor fluorophores at different places. When donor fluorophore is excited, acceptor quenches fluorescence emission of donor. This explains the efficiency of FRET assay in which emission of donor decreases while fluorescence of acceptor increases. Upon the temperature increase, denaturation process occurs due to destabilization of DNA in which the donor and acceptor ends get separated from each other (Carvalho & Cruz, 2020). In this project, BODIPY main body part is known to be able to bind to G-quadruplex regions and selected as G4 stabilizers (Uyar, Ozsamur, Celik, Ozbayram, & Erbas-Cakmak, 2023). Therefore, L1 and L2 compounds in the project were expected to bind to G-quadruplex structures and compound L3 used as control, they were tested with oligomers which are labelled at both ends with FAM and TAMRA fluorophores. As a result, the melting temperature of the oligomers were expected to be higher in the presence of the ligands due to stabilization of G4 regions. The FRET assay was performed by using fluorescently labelled G4 oligomers (*C-MYC*, *BCL-2*, *HIF1-A*, *H-TERT*, *C-KIT*) with measurement of RT-PCR device. FRET melting analysis was performed in 10 mM cacodylate buffer solution (10 mM sodium cacodylate trihydrate, 0.1 M LiCl) with 0.2 μM labeled fluorophores for compounds L1, L2 and L3 as 5 and 8 μM, respectively. This process was applied in RT-PCR device with 3 repetitions. The effect of G4 ligands on G4 region and melting curve were examined on samples with and without ligand.

3.3. Emission Measurements of Theranostic Ligand (L2)

Compound L2 is a theranostic agent which displays emission change upon binding to DNA G-quadruplex regions. The change of fluorescence intensity was measured by using RT-PCR in the presence and absence of oligomer. The compound L3 was used as control group which could not display efficient binding to G-quadruplex oligomer. In this analysis, compound L2 and L3 and were applied with and without FAM-TAMRA labeled c-myc oligomer (0.2 μM) as 8 μM in 10 mM cacodylate buffer solution (10 mM sodium cacodylate trihydrate, 0.1 M LiCl) FRET melting assay-like procedure was done. The difference in this method is that the initial temperature was kept at 25°C for 5 min, increased by 1°C every minute until reaching 37°C and the plate was read (FAM dye).

The range between 30-37°C is melting period. The experiment was performed as 3 repeats.

3.4. Cell Culture Experiments

In cell culture experiments, MFC-7 (human breast cancer cell line) cell line was used for all compounds (L1, L2 and L3 control). Cells were grown in High-Glucose DMEM (Dulbecco's Modified Eagle Medium) (4.5 g/L glucose, Sigma) containing 10% FBS (Fatal Bovine Serum, Gibco) and 0.1% Gentamicin (Sartorius) and incubated at 37°C 5% CO_2 for 24h (Nüve EC160 CO_2 incubator). They were used in MTT cell viability analysis, cell migration analysis and RNA extraction.

3.4.1. Cellular cytotoxicity assay (MTT)

MTT assay is the measurement of cell cytotoxicity by measuring mitochondrial activity of living cells. In mitochondria of living cells, yellow MTT substrate (3-(4,5-dimethylthiazol-2-yl)-2,5-diphenyltetrazolium bromide) is converted into purple colored formazan product. Formazan has crystal structure and is insoluble in water. DMSO is applied to solubilize crystals. Then the colorimetric change is detected by spectrophotometry methods and associated with cell number (Goodwin, 2007). In this assay, firstly MCF-7 cells were grown in high-glucose-DMEM medium containing 10% FBS, 0.1% gentamicin at 37°C in 5% CO_2 in the incubator for 24 h. Next day, they were treated with trypsin and collected. The collected cells were counted and cultured in a 96-well plate with $5x10^3$ cells per well in high glucose DMEM medium containing 10% FBS, 0.1% gentamicin as four replicates. Then cells were incubated at 37°C in 5% CO_2 in the incubator for 24 h. After 24 hours of incubation of the cells, the cell media was removed and compound L1 (0-2-4-8-16-32 μM) and compound L2 and L3 (0-20-40-80-160 μM) were applied to the new cell media as calculated ratio. The cells without agents containing only medium were used as control groups. L1, L2 and L3 stock solutions were prepared in DMSO and diluted with cell culture medium as 0.5 mM, 3 mM and 3 mM, respectively. Therefore, DMSO ratio in the medium was adjusted to not exceed 1%. After 24 hours of incubation, MTT solution was added (5 mg/mL stock solution) and incubated in the dark for 4 hours. At the end of the period, the medium was removed, and the formazan crystals were dissolved with DMSO. Spectrophotometric measurements were taken in the ELISA

plate reader at 570 nm. Concentration dependent cell death data was obtained by normalizing the results with the control groups. Statistical analysis of MTT assay was done by GraphPad software using ordinary one-way ANOVA.

3.4.2. Cell migration assay

In the previous study of Erbas-Cakmak research group, structurally similar G4 stabilizer ligand (GQ1, molecule 5 of this thesis) was demonstrated to influence cell migration of MCF-7 cells (Baser, 2023). This activity was checked for L1 whether it has the same effect or not. In this assay, MCF-7 cells were seeded on 24-well plate with a density of $7x10^4$ cells per well in 500 µL HG-DMEM culture medium supplemented with 10% FBS and 0.1 % gentamicin. The cells were incubated for 24 h at 37 °C in 5% CO_2 in the incubator. In 24 h, cells formed confluent monolayer, and a wound was introduced with a pipette tip gently. The L1 was dissolved in DMSO was added as solution to the culture medium at 5 and 10 µM doses and immediately washed with PBS to get rid of any dead cell or remaining due to scratching. Then, a scratch (wound) was created in the center of the wells with a pipette tip. Cell images were taken with an inverted light microscope (100 µm x 100 µm) at 0h, 24h and 48 h. Images were analysed using ImageJ software. In each group, change in area was normalized to initial wound area (0h) and then groups were compared to eliminate any discrepancies associated with initial wound shape.

3.4.3. RNA extraction from cancer cells

The mRNA expression level in ligand applied-MCF-7 cells (L1, L2 or L3) was analysed by quantitative reverse transcription polymerase chain reaction (RT-qPCR) method. Both L1 and L2 is thought to decrease gene expression level of G4 containing oncogenes. For this assay, RNAs were extracted from the cells by RNA isolation kit (Thermo Scientific, GeneJet, K0731). To do this, MCF-7 cells were collected by 500 µL trypsin and centrifuged at 800 rpm for 5 min. The proteinase K lysis buffer was added to the cells to break the cell membrane. To prepare the lysis buffer, 20 µL of β-mercaptoethanol is added per 1 ml of lysis buffer. The prepared lysis buffer was added as 600 µL to cell pellet and vortexed for 10 seconds. Then, 360 µL of 96% cold ethanol was added to the cell pellet and pipetted immediately after. The pellet was transferred to

filtered column and centrifuged at 12000 g for 1 min. The liquid phase was removed and precipitate was washed with 700 µL wash buffer 1 and centrifuged at 12000 g for 1 min. Then, the precipitate was washed with 600 µL wash buffer 2 and centrifuged at 12000 g for 1 min. This step was repeated with 250 µL wash buffer 2 at 12000 g for 1 min. Filtered columns are transferred to a new centrifuge tube, 50 µL of nuclease-free water was added and centrifuged at 12000 g for 1 min. The obtained RNA samples were stored at -80°C until needed. The concentration and purity of mRNAs was measured and checked by Nanodrop device **(**Migrodigital, Nabi UV/Vis nano spectrophotometer) at 260 nm. RNA quality is considered based on A260/A280 ratio which should be in the 1.8-2.0 range. Calculations for cDNA synthesis were done by using this data.

3.5. Detection of Gene Expression Level (RT-PCR)

Gene expression analysis was performed with cDNA samples obtained from mRNAs in the previous method. Before the gene expression analysis, cDNA synthesis was performed. The mRNAs were transformed into cDNAs with cDNA synthesis kit (Thermoscientific, High-Capacity cDNA Reverse Transcription Kit, 4368813). Firstly, 2X RT master mix was prepared based on the procedure in the manual. In each well, 2.0 µL of 10X RT buffer, 0.8 µL of 25X dNTP mix (100 mM), 2.0 µL of 10X RT random primers, 0.8 µL of MultiScribe™ Reverse Transcriptase enzyme and 4.2 µL of nuclease-free water was added. Then, 10 µL of RNA samples were added to each well and total volume is 20 µL. The manual procedure is started with 25°C for 10 min, 37°C for 120 min, 85°C for 5 min and hold at 4°C. At the end, 30 µl of nuclease-free water was added to the obtained cDNA samples and the volume was increased to 50 µl and stored at -20°C.

Gene expression analysis was performed with RT-qPCR (BioRad CFX96 Real-Time system C1000 Touch thermal cycler). The cDNA samples were analyzed according to specific primers (Sentebiolab) which are known to have G4 structures (Table 3.1). Gene expression analysis was performed with preparing master mix including SyberGreen (Nucleogene), primers and nuclease-free water. For each sample/well, 5 µL of SyberGreen, 0.5 µL of primers and 2.5 µL of nuclease-free water was mixed. 8 µL of the master mixture and 2 µL of cDNA samples were added in each well to reach 10 µL total volume. The RT-qPCR protocol is given in Table 3.1 below.

Table 3.1. RT-qPCR protocol based on Nucleogene manual

	Temperature (°C)	**Time**
1	95°C	15:00
2	95°C	00:15
3	60°C	00:30
	Plate reading	
4	Go to step 2, 45 cycles	
5	Melt curve 65°C to 95°C, increment 0.5°C + plate reading	00:05

The data analysis was done using a housekeeping gene *(B-ACTIN* or *GAPDH*) using the $2^{(-\Delta\Delta Ct)}$ method. Statistical analysis was performed using GraphPad one-way ANOVA. P values smaller than or equal to 0.05 are considered to be significant.

Table 3.2. Primer Sequences of Genes Required for RT-PCR Analysis

Gene	Forward Primer (5'-3')	Reverse Primer (5'-3')
GAPDH	GAA GGT GAA GGT CGG AGT C	GAA GAT GGT GAT GGG ATT TC
β-ACTIN	CAC CAT TGG CAA TGA GCG GTTC	AGG TCT TTG CGG ATG TCC ACG T
C-MYC	CCTGGTGCTCCATGAGGAGAC	CAGACTCTGACCTTTTGCCAGG
HIF1-α	TATGAGCCAGAAGAACTTTTAGGC	CACCTCTTTTGGCAAGCATCCTG
BCL-2	ATCGCCCTGTGGATGACTGAGT	GCCAGGAGAAATCAAACAGAGGC
GLUT1	GCTACAACACTGGAGTCATCAA	ACTGAGAGGGACCAGAGC
COX4-II	GAAGACGAGGGATGCACAG	GGCTCTTCTGGCATGGG
CDH-1	GCC TCC TGA AAA GAG AGT GGA AG	TGG CAG TGT CTC TCC AAA TCC G
PDK1	CATGTCACGCTGGGTAATGAGG	CTCAACACGAGGTCTTGGTGCA
WNT-1	CTGTCCTGCCTCCTCATC	GGACCCAGCACAATAAATAGTT
MMP-7	CCTCCACTCACTATGTAGA	ATTCTTATCTCCAACTTCCAA
VIM	AGGCAAAGCAGGAGTCCACTGA	ATCTGGCGTTCCAGGGACTCAT

3.6. Analysis of DNA Alkylation by L1

In this project, the chlorambucil-containing L1 molecule is produced with the intention to alkylate DNA together with G4 stabilization through the nucleophilic substitution reaction. Denaturing urea polyacrylamide gel electrophoresis (urea-PAGE) was used to detect DNA alkylation. The oligonucleotides to be determined by treating with L1 agent (100 μM) were selected as c-myc, and dsDNA and -‘5FAM and -3’TAMRA labeled c-myc and dsDNA oligonucleotides (5 μM). dsDNA was used as a control. L1 agent was treated with the selected oligonucleotides and incubated at 37°C for 24 hours (Nüve EC160 CO_2 incubator). For the gel containing 40% polyacrylamide (29:1 acrylamide-bisacrylamide), 8M urea (Sigma-Aldrich, U5378) and 1X Tris-Borate-EDTA (TBE) buffer solution, N,N,N,N’-tetramethylethylenediamine (TEMED) (Sigma-Aldrich, T7024) and 30% ammonium per sulfate solution (Sigma-Aldrich, A3678) was used. For urea-PAGE gel, electrophoresis gel running glass apparatus was used (BioRad Mini-PROTEAN® Tetra Handcast Systems). When the gel is ready, 3 μL of dye (Thermo Fisher Scientific, TriTrack 6X) was added to 3 μL samples containing previously prepared oligonucleotide and added into the wells. To determine the size of the bands, 100-bp DNA ladder (Thermo Fisher Scientific, SM0321) was used as a marker. The prepared urea-PAGE gel was run at 80 voltage in 1X TBE running buffer for gel electrophoresis. Visualization of gel was performed by adding SafeView™ Classic dye (abm, G108) to the gel mixture. Images were obtained using Alexa filters (BioRad, ChemiDoc Imaging System 12003153) for gel imaging.

4. RESULTS AND DISCUSSION

4.1. Synthesis of Compounds

The characterization of all compounds synthesized throughout the project was determined by ^{1}H NMR, ^{13}C NMR and/or HRMS. ^{1}H NMR and ^{13}C NMR spectrums (Varian Inova instrument, 400 MHz) were obtained in Science and Technology Research and Application Center (BİTAM) at Necmettin Erbakan University. The mass spectroscopy (HRMS) analyses (Agilent 6530 Accurate-Mass Q-TOF LC/MS (ESI)) were performed at Erzurum Atatürk University Eastern Anatolian High Technology Research and Application Center (DAYTAM). Characterization data of all compounds were given in 1-22 appendices. All chemicals, cell culture ingredients used in this study were purchased from commercial companies. The column chromatography used with silica gel stationary phase (230–400 mesh, SiliCycle Inc., Canada) was applied in purification of synthesized compounds.

4.2. FRET Melting Assay

FRET melting assay was done with different molecules (L1, L2 and L3- control) at different concentrations 5 μM and 8 μM, respectively. In this assay, compound that were designed as G-quadruplex ligands display efficient binding to G4 structures on labelled oligomers and negligible binding to dsDNA (Figure 4.1 and 4.2). The synthesized ligands can provide significant stabilization in c-myc, bcl-2 and H-telo oligomers forming G-quadruplex. T_m (melting temperature) is increased as 35°C in c-myc, 22°C in bcl-2 and 28°C in h-telo oligomers (Figure 4.1). Also, L2 enables stabilization of G4 structure in c-myc oligomer by increasing T_m up to 10°C (Figure 4.2). This increase also demonstrates the effect of alkylation in G4 stabilization when compared to GQ1 study (Baser et al., 2023).

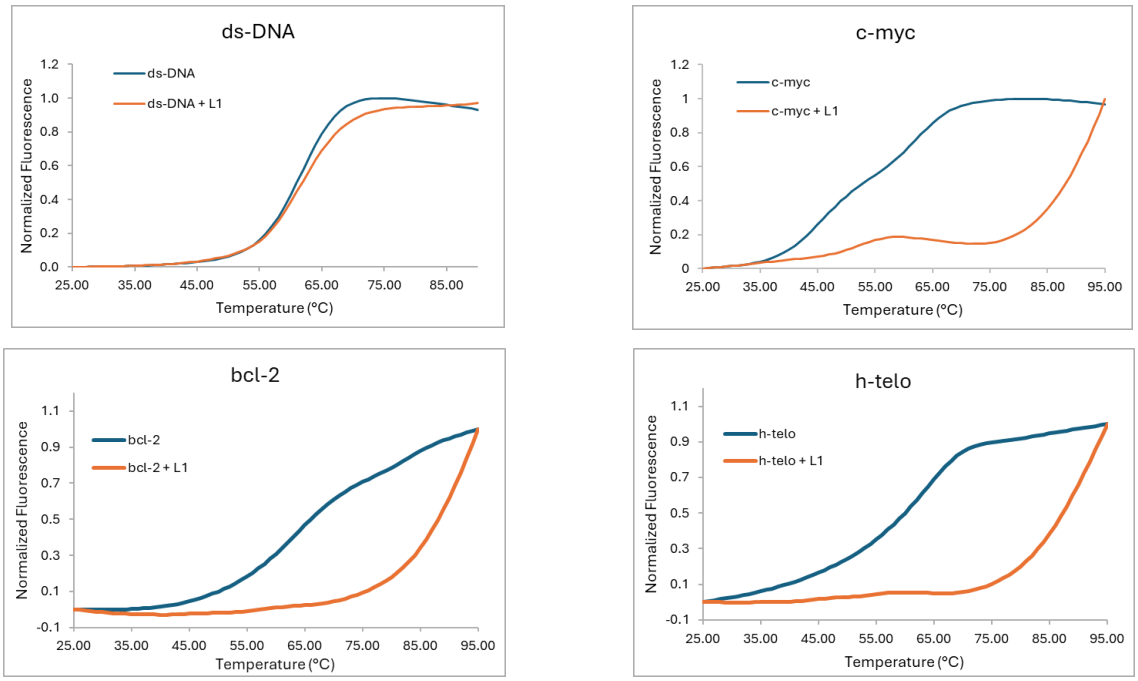

Figure 4.1. FRET Melting Assay results of compound L1. Labelled oligomers (ds-DNA, c-myc, bcl-2 and h-telo) as 0.2 µM in the presence and absence of L1 (5 µM), n=3

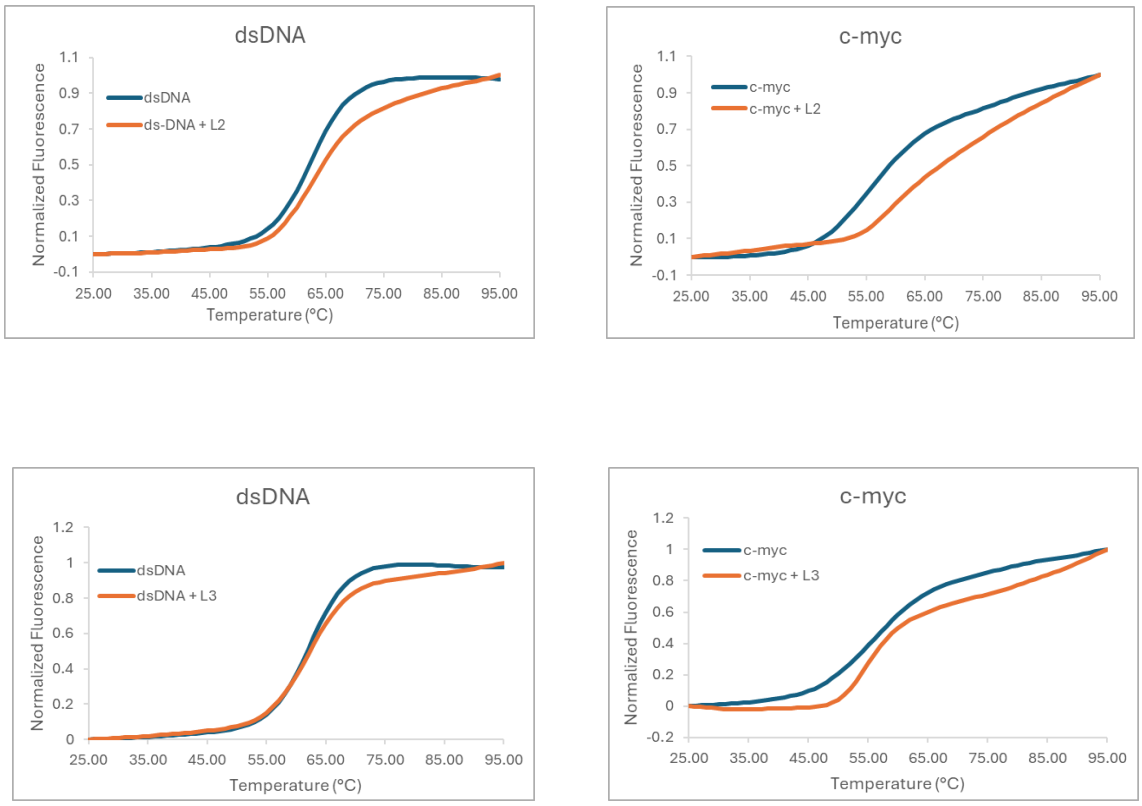

Figure 4.2. FRET melting assay results of compound L2 (top) and L3 (bottom). Labelled oligomers (ds-DNA and c-myc) as 0.2 µM in the presence and absence of L2 and L3 (8 µM), n=3

The compound L3 was used as control and presence of only pyridinium BODIPY on the structure cannot provide enough stabilization of G4. While the L2 compound containing anthracene and triazolium is a more selective and effective ligand.

4.3. Emission Measurements of Theranostic Ligand (L2)

The effect of emission change of ligand L2 (8 µM) was measured by RT-qPCR device in the presence and absence of the c-myc oligomer which contains G4 structure. When oligomer having G4 region was applied to the L2 solution the emission change could be observed. This explains the effect of L2 binding to G4 structure resulting in change of emission (Figure 4.3a). The compound L3 did not display a same emission profile therefore triazolium and/or anthracene units seems to be important for this behaviour (Figure 4.3b). Also, it was observed that, the ligand L2 fluorescence emission response was increased upon concentration increase of c-myc oligomer (0.15-1.2 µM) both in anthracene and BODIPY site of the structure (Figure 4.3c and 4.3d).

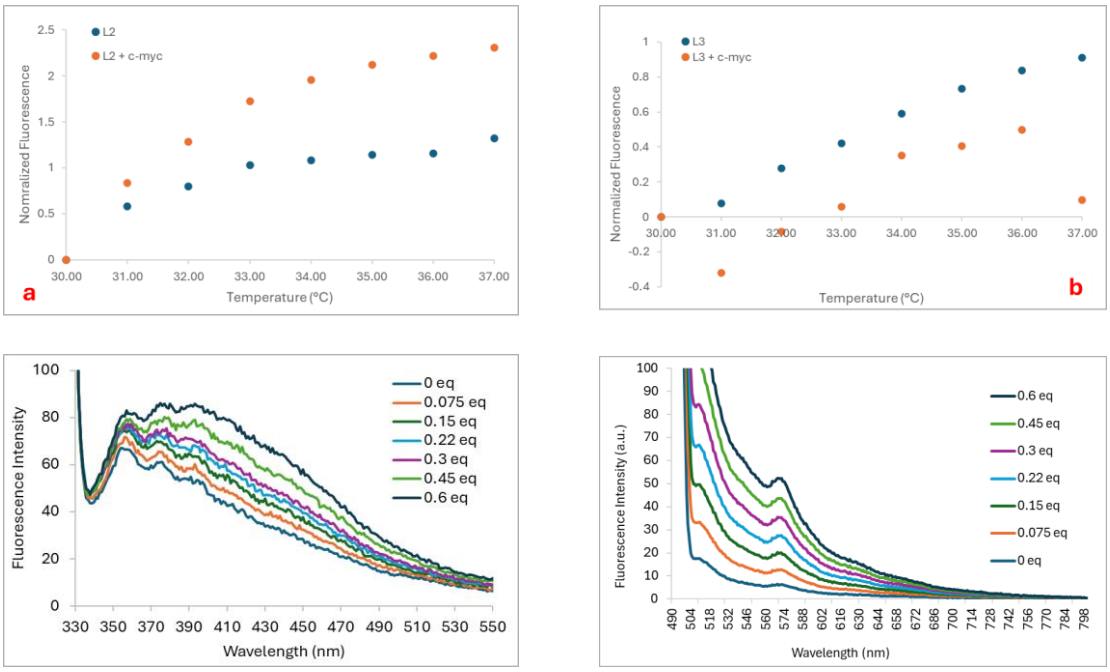

Figure 4.3. The emission measurement by RT-PCR upon binding to G4 structures. Change in the emission of **(a)** compound L2 **(b)** compound L3 in the presence of c-myc oligomer. (c) Emission measurement of anthracene site of L2 upon increase concentration of c-myc (d) Emission measurement of BODIPYsite of L2 upon increase concentration of c-myc (0.15-1.2 µM).

4.4. Cell Culture Experiments

All cell culture experiments were performed with MCF-7 cell line grown in HG-DMEM cell medium containing 10% FBS and 0.1% Gentamicin. As part the of cell culture experiments, MTT cell viability analysis, cell migration analysis and RNA extraction were conducted. Results of analyses were given below.

4.4.1. Cellular cytotoxicity assay (MTT)

MCF-7 cells were seeded in a 96-well plate with $5x10^3$ cells per well in HG-DMEM medium containing 10% FBS, 0.1% gentamicin. Four replicates were made for each experimental group. 6 doses of L1 were used in MTT experiments (0-2-4-8-16-32 µM) as shown in Figure 4.3. The most significant difference observed between control and last concentrations (16 and 32 µM) has a p value which is smaller than 0.0001. The IC_{50} value of L1 was calculated as 34.316 µM (Figure 4.4).

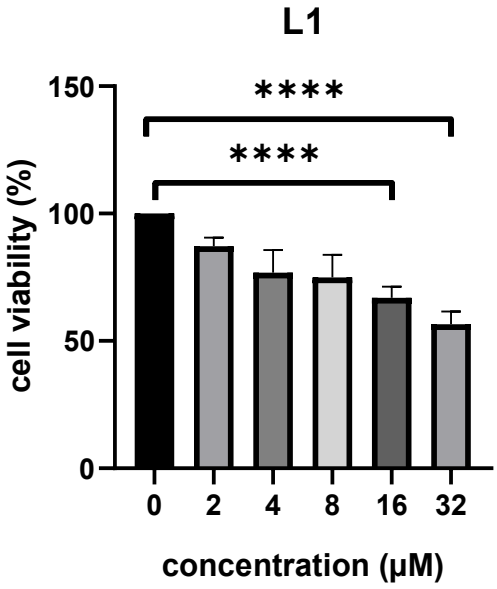

Figure 4.4. Results of MTT cell viability analysis of the compound L1 for MCF-7 cell line, n=4, **** $p<0.0001$

0-20-40-80-160 μM of L2 and L3 were used for MTT analysis as shown in Figure 4.5 and 4.6. Compound L2 showed no significant toxicity up to 80 μM even though it could bind to G4 structures at as low as 8 μM (Figure 4.5). The IC_{50} value of L2 was calculated as 80.35 μM. However, the compound L3 did not have shown significant toxicity and cell viability was higher in almost all doses until 160 μM (Figure 4.6). Therefore, the IC_{50} value of L3 is calculated to be greater than 160 μM. All analyses were done with GraphPad Prism software using ordinary one-way ANOVA test.

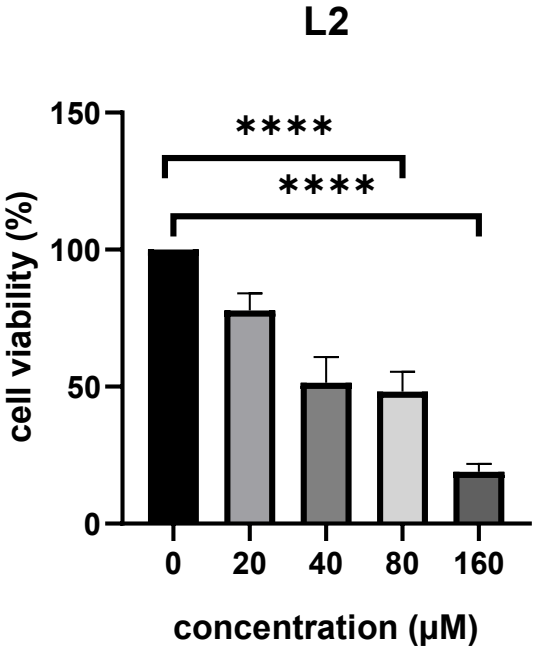

Figure 4.5. Results of the MTT cell viability analysis of compound L2 for MCF-7 cell line, n=4, **** $p<0.0001$

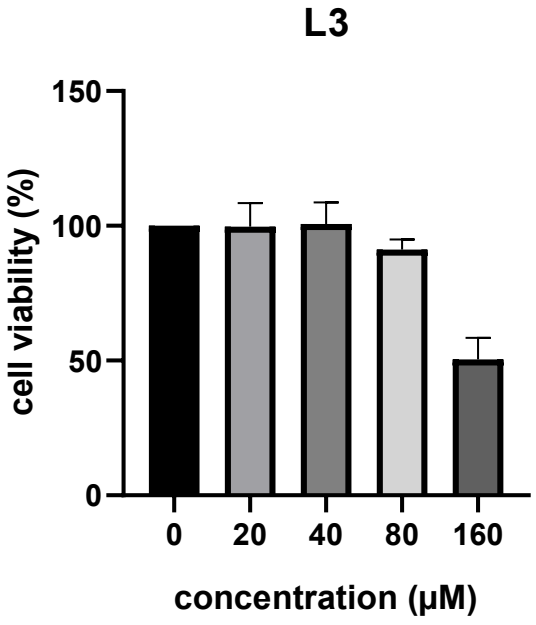

Figure 4.6. Results of the MTT cell viability analysis of compound L3 for MCF-7 cell line, n=4.

4.4.2. Cell migration analysis

Antimetastatic ability of compound L1 was tested in MCF-7 cells through analysis of cell migration. MCF-7 cells were seeded on 24-well plate as $7x10^4$ cells per well in 500 µL HG-DMEM culture medium supplemented with 10% FBS and 0.1 % gentamicin. Cell images were obtained through 48h. Two different doses (5 µM and 10 µM) of L1 were used, each with three replicates. Cell images were taken for every 24h starting from the beginning (t=0) by light microscope (Figure 4.7). As a result, there is a significant difference in percent wound closure between control and 10 µM ligand applied cells especially in 48h time period. Ligand L1 has proven to have inhibitory effect on cell migration as GQ1 (Baser et al., 2023).

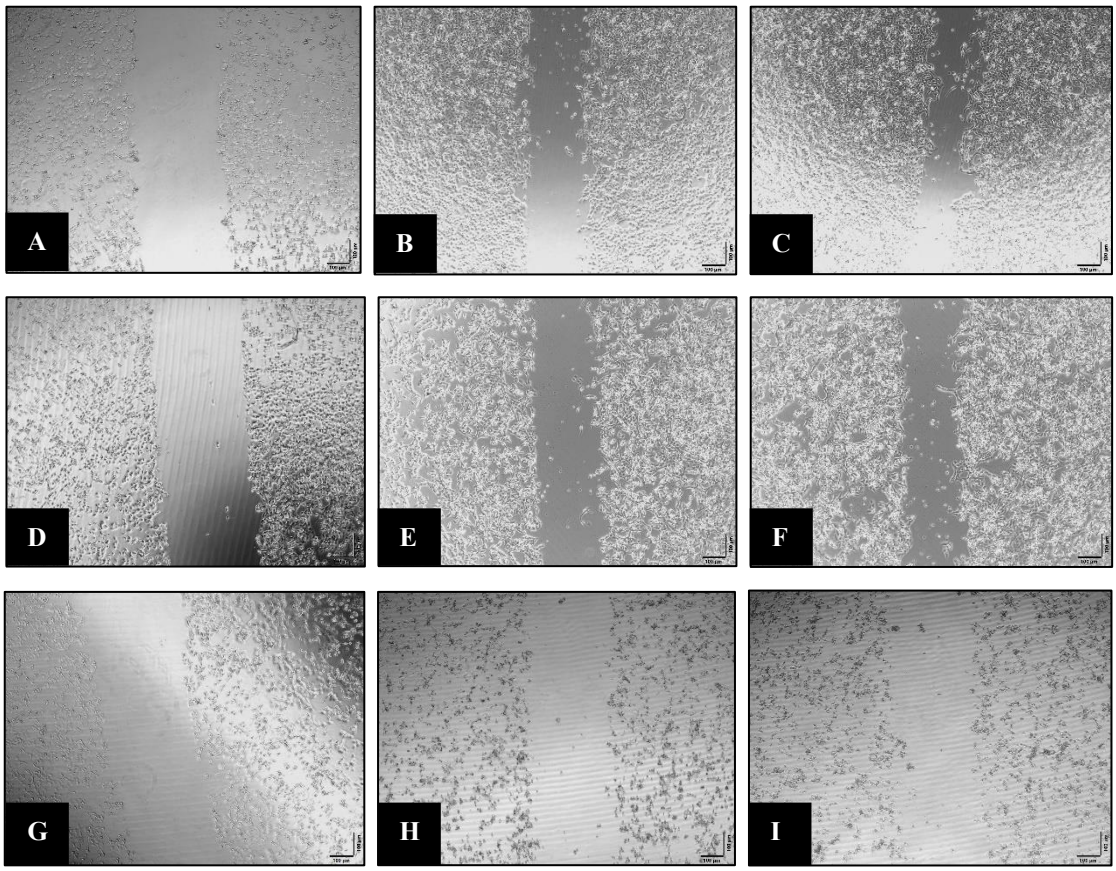

Figure 4.7. Cell images obtained from cell migration assay when 5 and 10 µM of compound L1 was applied to MCF-7 cell line. **A-C)** control group 0-24-48h. **D-F)** L1 (5 µM) 0-24-48h. **G-I)** L1 (10 µM) 0-24-48h.

Wound areas were calculated with ImageJ software and statistical analyses were done by GraphPad One-way ANOVA shown in figure 4.8.

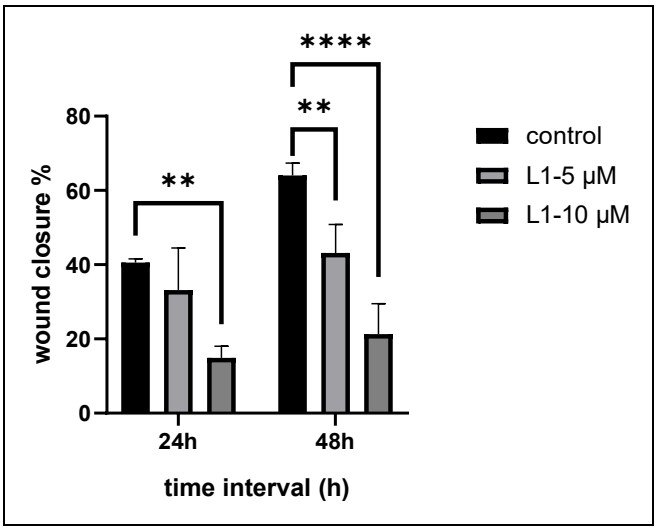

Figure 4.8. Statistical analysis of percent wound closure of L2 ligand-applied MCF-7 cells. n=3, **** $p<0.0001$

4.4.3. Analysis of gene expression

Synthesized ligands were applied MCF-7 cells, RNA is isolated to obtain cDNA for gene expression analyses. Therefore, cells were grown and seeded into 6-well plates for extraction of RNA first by RNA isolation kit (Thermo Scientific, GeneJet, K0731) and then transformed into cDNA by using cDNA synthesis kit (Thermoscientific, High-Capacity cDNA Reverse Transcription Kit, 4368813). DNAs obtained in sufficient purity and concentration were stored at -20 degrees to be used in gene expression analyses.

Gene expression level was examined for genes that have G-quadruplex structures in their promoter site or proximal sites as stated in Table 3.1. The ligand L1 was tested with *C-MYC*, *COX-4-II*, *GLUT-1*, *HIF-1A*, *PDK-1* and *WNT-1* genes shown in figure 4.9. The compound L1 caused a decrease in expression of *PDK-1*, *COX-4-II*, *HIF-1A* and *C-MYC* genes in 5 μM. This means that compound L1 could suppress some oncogenes that have important roles in many cellular signalling pathways such as cell metabolism, proliferation, cell survival, angiogenesis, electron transport chain, cellular respiration, tumour metabolism, etc. On the other hand, compound L1 increased gene expression level of *WNT-1* which is important in cell proliferation in cellular metabolism. The interesting point here is that when L1 is applied, *HIF-1A* gene expression is suppressed while *GLUT-1* gene expression, which is directly related to *HIF-1A*, was not affected (Figure 4.9).

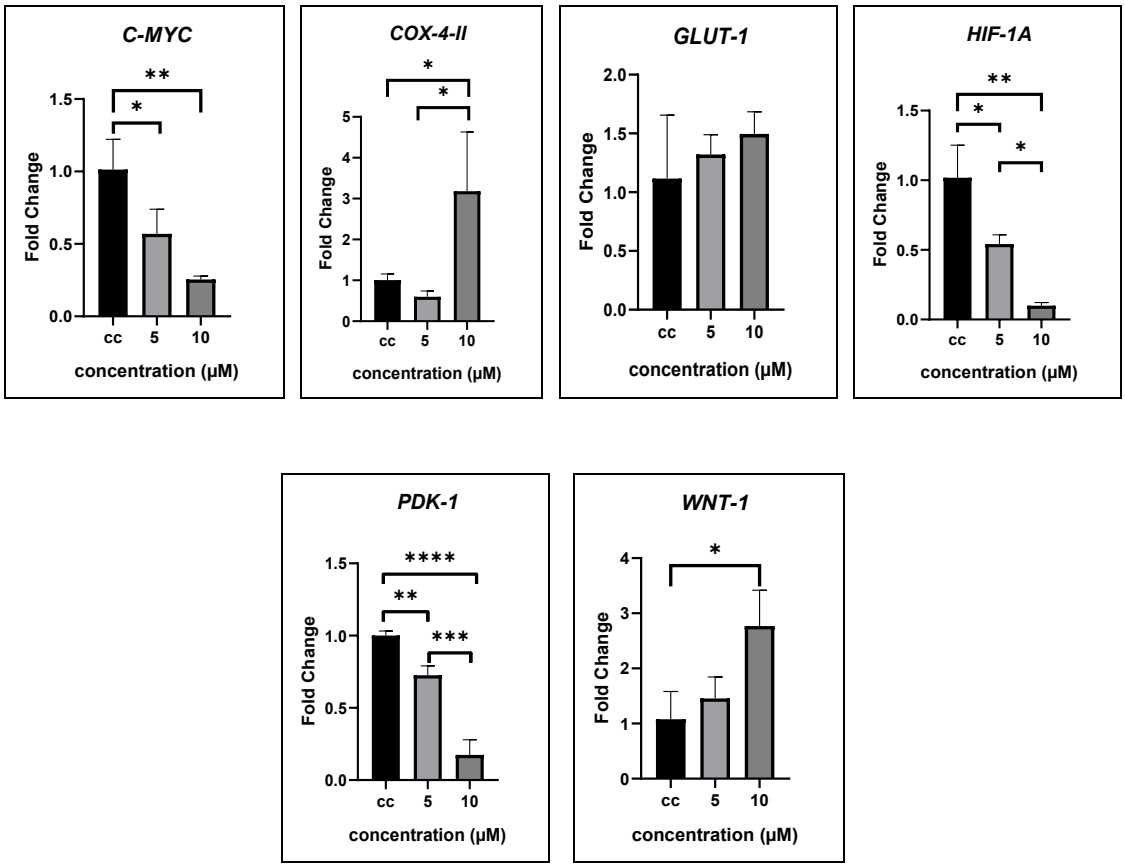

Figure 4.9. Results of RT-qPCR analysis of gene expression changes in MCF-7 cells treated with L1 compound at 5 and 10 μM doses, n=3, **** p<0.0001

The compound L2 and L3 were applied on MCF-7 cells as 15 and 30 μM doses. The expression level of *BCL-2*, *C-MYC* and *HIF-1A* was suppressed by compound L2 efficiently (Figure 4.10). The compound L3 was used as control group. However, it could also suppress gene expression at 15 μM in those oncogenes. This indicates that BODIPY main body could bind to G-quadruplex regions and cause change in gene expression level (Figure 4.11). Compared to previously reported chlorambucil free G4 ligand with the same structure, L1 display much more enhanced reduction in the expression of *PDK-1* and *HIF-1A*, and also expression of *COX-4II*. This indicates dual effect, namely alkylation and G4 stabilization, may have better therapeutic effect.

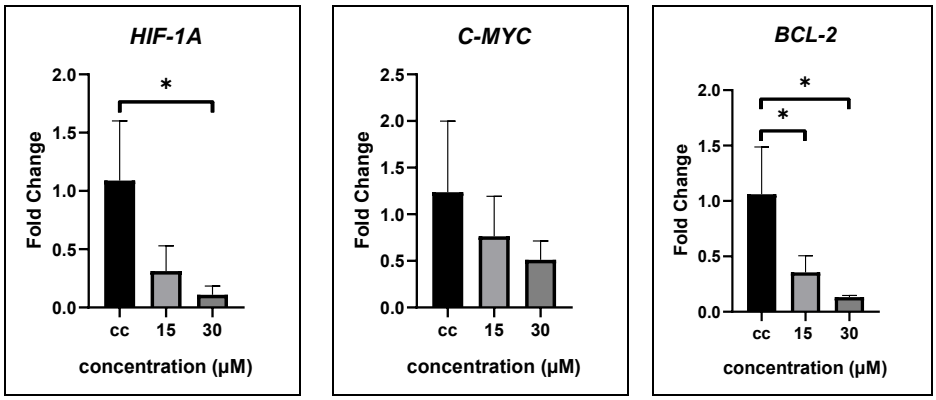

Figure 4.10. Results of RT-qPCR analysis of gene expression changes in MCF-7 cells treated with compound L2 at 15 and 30 μM doses, n=3, $p<0.05$

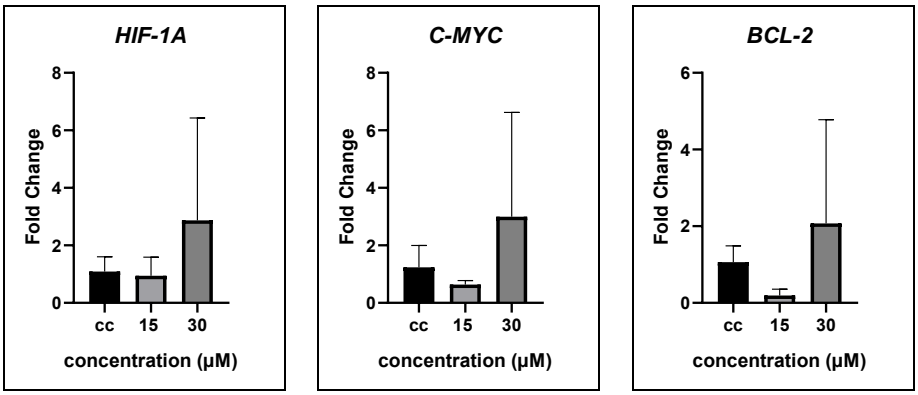

Figure 4.11. Results of RT-qPCR analysis of gene expression changes in MCF-7 cells treated with L3 compound at 15 and 30 μM doses, n=3, $p>0.9$

4.5. Detection of DNA Alkylation by L1

The DNA alkylation induced by compound L1 was analysed by urea-PAGE gel method with FAM and TAMRA labelled ds-DNA and c-myc oligomers (5 μM). To analyse alkylation, higher concentration of L1 was used (100 μM). In agent containing wells, the bands appeared faint. However, in wells without agent, bands appeared as bright. The gel image is shown in figure 4.12. The decrease in the signal obtained from the band in the agent-containing samples was attributed to the quenching of the emission of FAM/TAMRA labels due to alkylation or binding. The BODIPY compounds such as L1 structure, have absorbance in the region of 650 nm or above and have the potential to quench the emission of FAM or TAMRA. The quenching is observed in both c-myc and ds-DNA and this result is attributed to non-specific binding at high concentrations. On the other hand, samples treated with unlabelled c-myc (2.5 μM) and dsDNA L1 (50 μM)

were incubated for 72 hours at 37°C and sent to Erzurum Atatürk University (DAYTAM) for mass analysis. However, no peaks were obtained due to the small sample size and high oligomer masses. Mass analyses of small fragments could not be detected due to low signal intensities or degradation during the sample transfer.

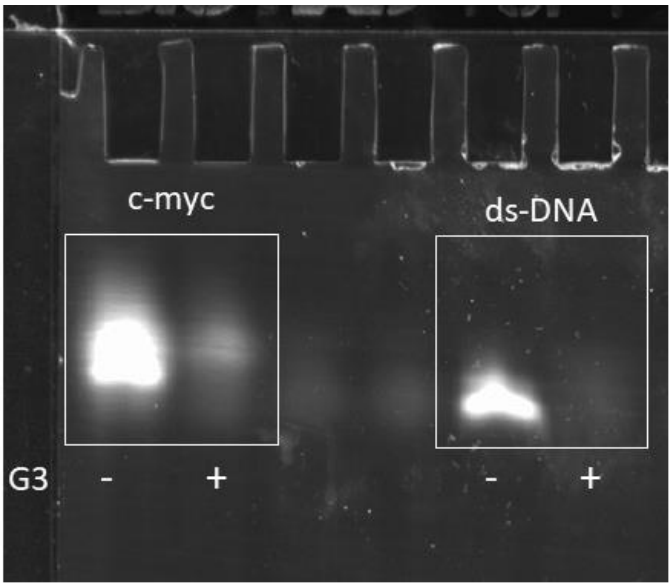

Figure 4.12. The gel electrophoresis image of labelled c-myc and ds-DNA oligomer samples treated with L1 (100 μM).

5. CONCLUSIONS AND RECOMMENDATIONS

5.1 Results

In this thesis, two BODIPY-based novel G-quadruplex ligands were developed which are shown to regulate the expression of oncogenes that have G4 structures on MCF-7 cancer cells. Some of the oncogenes such as *GLUT-1* and *WNT-1* expression levels are shown to be increased upon L1 binding. This could be associated with DNA alkylation effect of L1 ligand. The compound L2 could effectively suppress *HIF-1A*, *C-MYC* and *BCL-2* expression levels. The ligand may bind to DNA G4 region through both BODIPY and anthracene units. Moreover, it was observed that these two fluorescent units (BODIPY and anthracene) displayed emission change upon binding to G4 region. This demonstrates that the theranostic agent could work well by exhibiting both suppression of oncogenes (therapeutic) and fluorescence intensity change (diagnostic). Also, it was shown that only BODIPY cationic moiety cannot sufficiently bind to G4 structures, and it requires higher concentration for G4 binding while at higher concentrations binding to non-G4 including ds-DNA is becoming a risk.

5.2 Recommendations

The compounds designed and synthesized in this thesis work can further be optimized structurally to enable selectivity. The reason is that none of these ligands are selective according to cell type or can be activated by external effects (they are already in active form) means that they can bind to G4 structures in healthy cells as well. Therefore, new generation ligands can be designed to be more selective by adding functional groups or cleavable units upon external stimuli (heat, pH, light, enzymes etc.). The ligand L2 has a cationic station like an axle of a rotaxane molecular machine. As a result, these structures can be modified to have interlocked, functionally advanced forms. Also, to understand the interaction of designed ligands with G4 structures, different cell lines could be used with different genes to better evaluate the role in metabolic regulation.

6. REFERENCES

Ahmad, H., Muhammad, S., Mazhar, M., Farhan, A., Iqbal, M. S., Hiria, H., Yu, C., Zhang, Y., & Guo, B. (2025). Unveiling cellular mysteries: Advances in BODIPY dyes for subcellular imaging. *Coordination Chemistry Reviews, 526*, 216383. doi:https://doi.org/10.1016/j.ccr.2024.216383

Alessandrini, I., Recagni, M., Zaffaroni, N., & Folini, M. (2021). On the road to fight cancer: The potential of G-quadruplex ligands as novel therapeutic agents. *International journal of molecular sciences, 22*(11), 5947.

Balasubramanian, S., Hurley, L. H., & Neidle, S. (2011). Targeting G-quadruplexes in gene promoters: a novel anticancer strategy? *Nature Reviews Drug Discovery, 10*(4), 261-275.

Banerjee, N., Panda, S., & Chatterjee, S. (2022). Frontiers in G-Quadruplex therapeutics in cancer: Selection of small molecules, peptides and aptamers. *Chemical Biology & Drug Design, 99*(1), 1-31.

Baser, A., Basar, B., Dogan, H. B., Sener, G., Ozsamur, N. G., Celik, F. S., Altves, S., & Erbas-Cakmak, S. (2023). Reprograming cancer cells by a BODIPY G-quadruplex stabiliser. *Chemical Communications, 59*(83), 12447-12450.

Biffi, G., Tannahill, D., Miller, J., Howat, W. J., & Balasubramanian, S. (2014). Elevated levels of G-quadruplex formation in human stomach and liver cancer tissues. *PloS one, 9*(7), e102711.

Bochman, M. L., Paeschke, K., & Zakian, V. A. (2012). DNA secondary structures: stability and function of G-quadruplex structures. *Nature Reviews Genetics, 13*(11), 770-780.

Boyer, A.-S., Grgurevic, S., Cazaux, C., & Hoffmann, J.-S. (2013). The human specialized DNA polymerases and non-B DNA: vital relationships to preserve genome integrity. *Journal of Molecular Biology, 425*(23), 4767-4781.

Brooks, T. A., Kendrick, S., & Hurley, L. (2010). Making sense of G-quadruplex and i-motif functions in oncogene promoters. *The FEBS journal, 277*(17), 3459-3469.

Carvalho, J., & Cruz, C. (2020). Forster resonance energy transfer for studying nucleic acids denaturation: A chemical and biological sciences laboratory experiment. *Biochemistry and Molecular Biology Education, 48*(4), 329-336. doi:https://doi.org/10.1002/bmb.21353

Choi, J., & Majima, T. (2011). Conformational changes of non-B DNA. *Chemical Society reviews, 40*(12), 5893-5909.

De Cian, A., Cristofari, G., Reichenbach, P., De Lemos, E., Monchaud, D., Teulade-Fichou, M. P., Shin-Ya, K., Lacroix, L., Lingner, J., & Mergny, J. L. (2007). Reevaluation of telomerase inhibition by quadruplex ligands and their

mechanisms of action. *Proc Natl Acad Sci U S A, 104*(44), 17347-17352. doi:10.1073/pnas.0707365104

Di Antonio, M., McLuckie, K. I., & Balasubramanian, S. (2014). Reprogramming the mechanism of action of chlorambucil by coupling to a G-quadruplex ligand. *J Am Chem Soc, 136*(16), 5860-5863. doi:10.1021/ja5014344

Figueiredo, J., Mergny, J.-L., & Cruz, C. (2024). G-quadruplex ligands in cancer therapy: Progress, challenges, and clinical perspectives. *Life Sciences, 340*, 122481.

Gellert, M., Lipsett, M. N., & Davies, D. R. (1962). Helix formation by guanylic acid. *Proceedings of the National Academy of Sciences, 48*(12), 2013-2018.

Goodwin, A. M. (2007). In vitro assays of angiogenesis for assessment of angiogenic and anti-angiogenic agents. *Microvascular Research, 74*(2), 172-183. doi:https://doi.org/10.1016/j.mvr.2007.05.006

Guan, L., Zhou, Y., Li, X., Mao, Y., Li, A., Fu, Y., Liu, W., Dong, S., Liang, Z., & Zhang, Y. (2023). ON–OFF fluorescent cyanine dye based on a benzothiophenyl rotor enables selective illumination of G-quadruplexes in mitochondria. *Analytical Chemistry, 95*(24), 9288-9296.

Henderson, E., Hardin, C. C., Walk, S. K., Tinoco Jr, I., & Blackburn, E. H. (1987). Telomeric DNA oligonucleotides form novel intramolecular structures containing guanine· guanine base pairs. *Cell, 51*(6), 899-908.

Kosiol, N., Juranek, S., Brossart, P., Heine, A., & Paeschke, K. (2021). G-quadruplexes: a promising target for cancer therapy. *Molecular Cancer, 20*, 1-18.

Kumar, P. P. P., Saxena, S., & Joshi, R. (2025). BODIPY Dyes: A New Frontier in Cellular Imaging and Theragnostic Applications. *Colorants, 4*(2), 13.

Makova, K. D., & Weissensteiner, M. H. (2023). Noncanonical DNA structures are drivers of genome evolution. *Trends in Genetics, 39*(2), 109-124. doi:10.1016/j.tig.2022.11.005

Mendoza, O., Bourdoncle, A., Boulé, J.-B., Brosh Jr, R. M., & Mergny, J.-L. (2016). G-quadruplexes and helicases. *Nucleic Acids Research, 44*(5), 1989-2006.

Mirsky, A. E. (1968). The discovery of DNA. *Scientific American, 218*(6), 78-90.

Mishra, S. K., Jain, N., Shankar, U., Tawani, A., Sharma, T. K., & Kumar, A. (2019). Characterization of highly conserved G-quadruplex motifs as potential drug targets in Streptococcus pneumoniae. *Scientific Reports, 9*(1), 1791.

Nakanishi, C., & Seimiya, H. (2020). G-quadruplex in cancer biology and drug discovery. *Biochemical and Biophysical Research Communications, 531*(1), 45-50.

Neidle, S. (2017). Quadruplex nucleic acids as targets for anticancer therapeutics. *Nature Reviews Chemistry, 1*(5), 0041.

Nicolson, F., & Kircher, M. F. (2021). Theranostics: Agents for Diagnosis and Therapy. In *Molecular Imaging* (pp. 655-677): Elsevier.

Palma, E., Carvalho, J., Cruz, C., & Paulo, A. (2021). Metal-based G-quadruplex binders for cancer theranostics. *Pharmaceuticals, 14*(7), 605.

Sanchez-Martin, V., Lopez-Pujante, C., Soriano-Rodriguez, M., & Garcia-Salcedo, J. A. (2020). An updated focus on quadruplex structures as potential therapeutic targets in cancer. *International journal of molecular sciences, 21*(23), 8900.

Shay, J. W., & Wright, W. E. (2019). Telomeres and telomerase: three decades of progress. *Nature Reviews Genetics, 20*(5), 299-309.

Shinziya, H., Menon, R. S., & Das, A. K. (2024). A rapid investigation of near-infrared (NIR) fluorescent switch-on probes for detection and in cellulo tracking of G-quadruplex and double-stranded DNA. *RSC advances, 14*(42), 30631-30646.

Suseela, Y. V., Satha, P., Murugan, N. A., & Govindaraju, T. (2020). Recognition of G-quadruplex topology through hybrid binding with implications in cancer theranostics. *Theranostics, 10*(23), 10394.

Uyar, B., Ozsamur, N. G., Celik, F. S., Ozbayram, I., & Erbas-Cakmak, S. (2023). Downregulation of gene expression in hypoxic cancer cells by an activatable G-quadruplex stabiliser. *Chemical Communications, 59*(16), 2247-2250. doi:10.1039/D2CC06347F

Wojtyla, A., Gladych, M., & Rubis, B. (2011). Human telomerase activity regulation. *Molecular biology reports, 38*, 3339-3349.

Zhang, L., Liu, X., Lu, S., Liu, J., Zhong, S., Wei, Y., Bing, T., Zhang, N., & Shangguan, D. (2020). Thiazole orange styryl derivatives as fluorescent probes for G-quadruplex DNA. *ACS Applied Bio Materials, 3*(5), 2643-2650.

Zhang, P. L., Wang, Z. K., Chen, Q. Y., Du, X., & Gao, J. (2019). Biocompatible G-Quadruplex/BODIPY assembly for cancer cell imaging and the attenuation of mitochondria. *Bioorg Med Chem Lett, 29*(15), 1943-1947. doi:10.1016/j.bmcl.2019.05.043

APPENDIX

Appendix-1 ^{1}H NMR spectrum of compound 6 (400 MHz, $CDCl_3$).

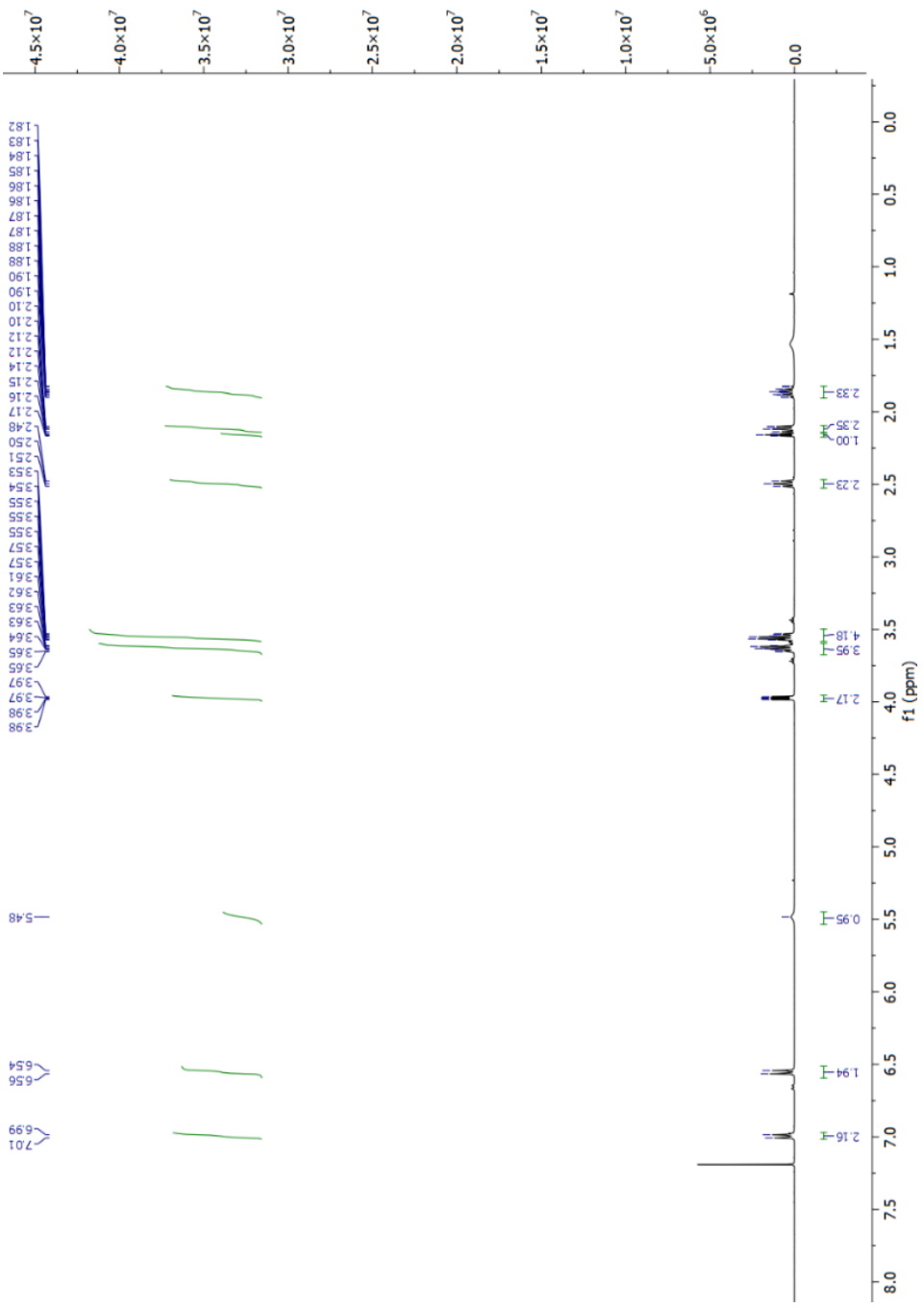

Appendix-2 ^{13}C NMR Spectrum of compound 6 (101 MHz, $CDCl_3$).

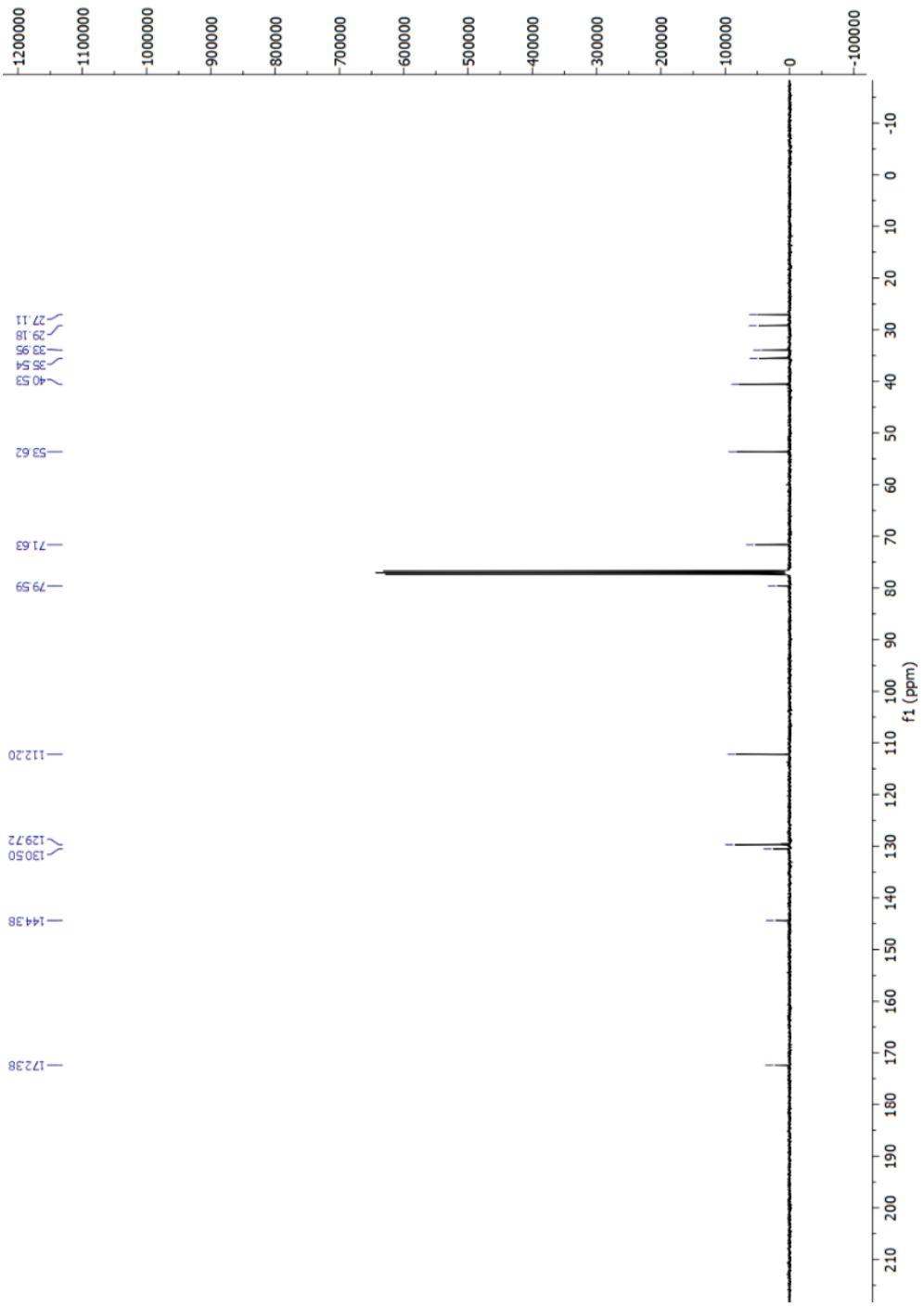

Appendix-3 HRMS Spectrum of compound 6

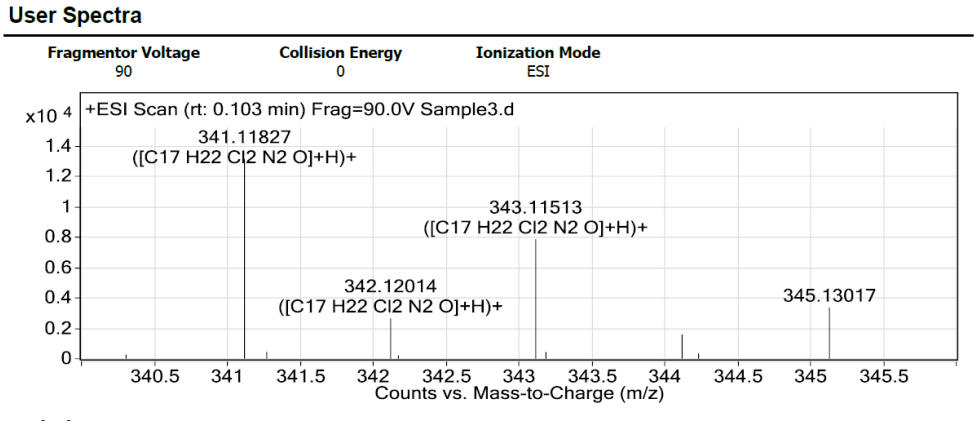

Appendix-4 ^{1}H NMR spectrum of compound L1 (400 MHz, $CDCl_3$).

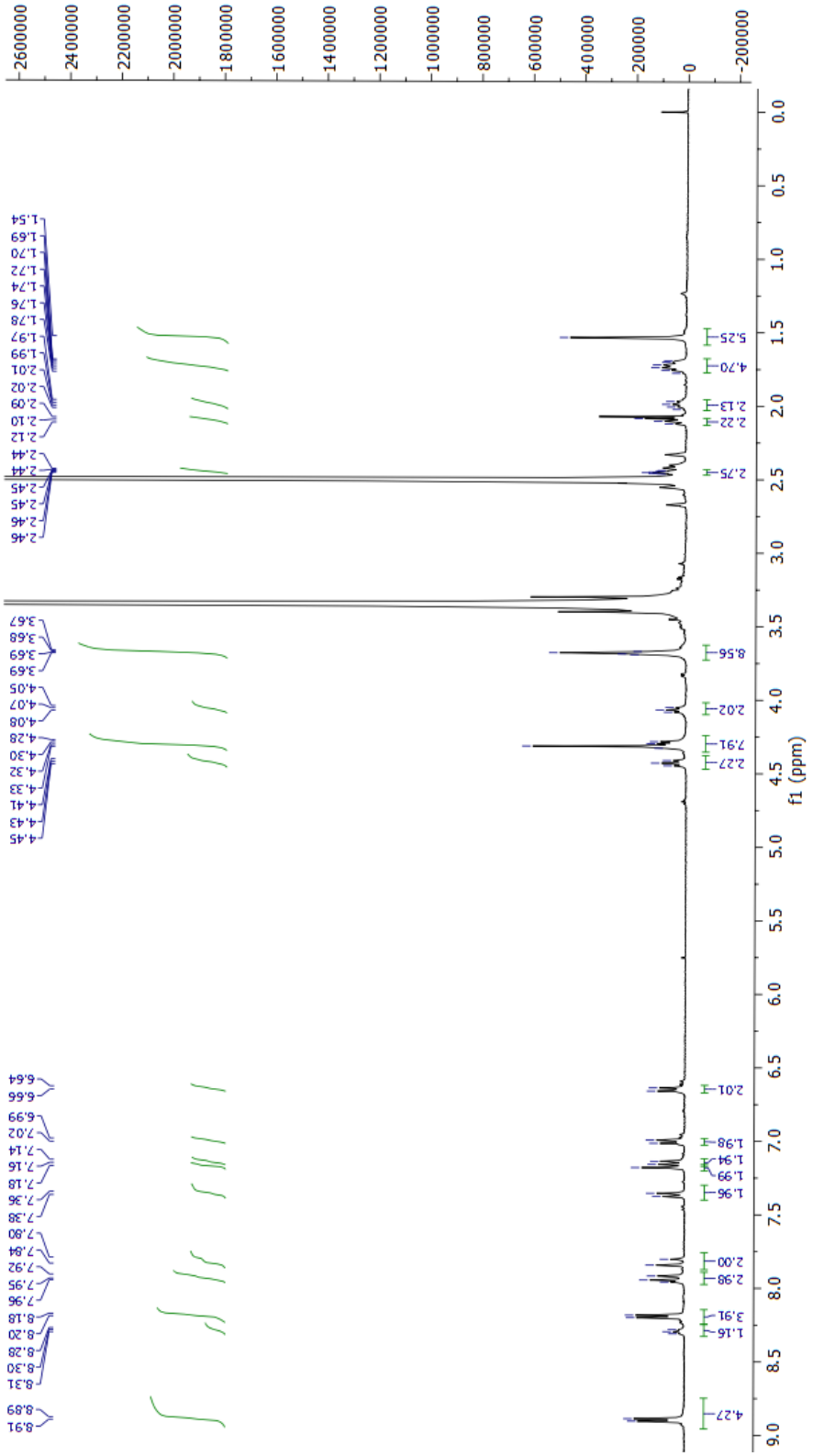

Appendix-5 ^{13}C NMR Spectrum of compound L1 (101 MHz, DMSO-d_6).

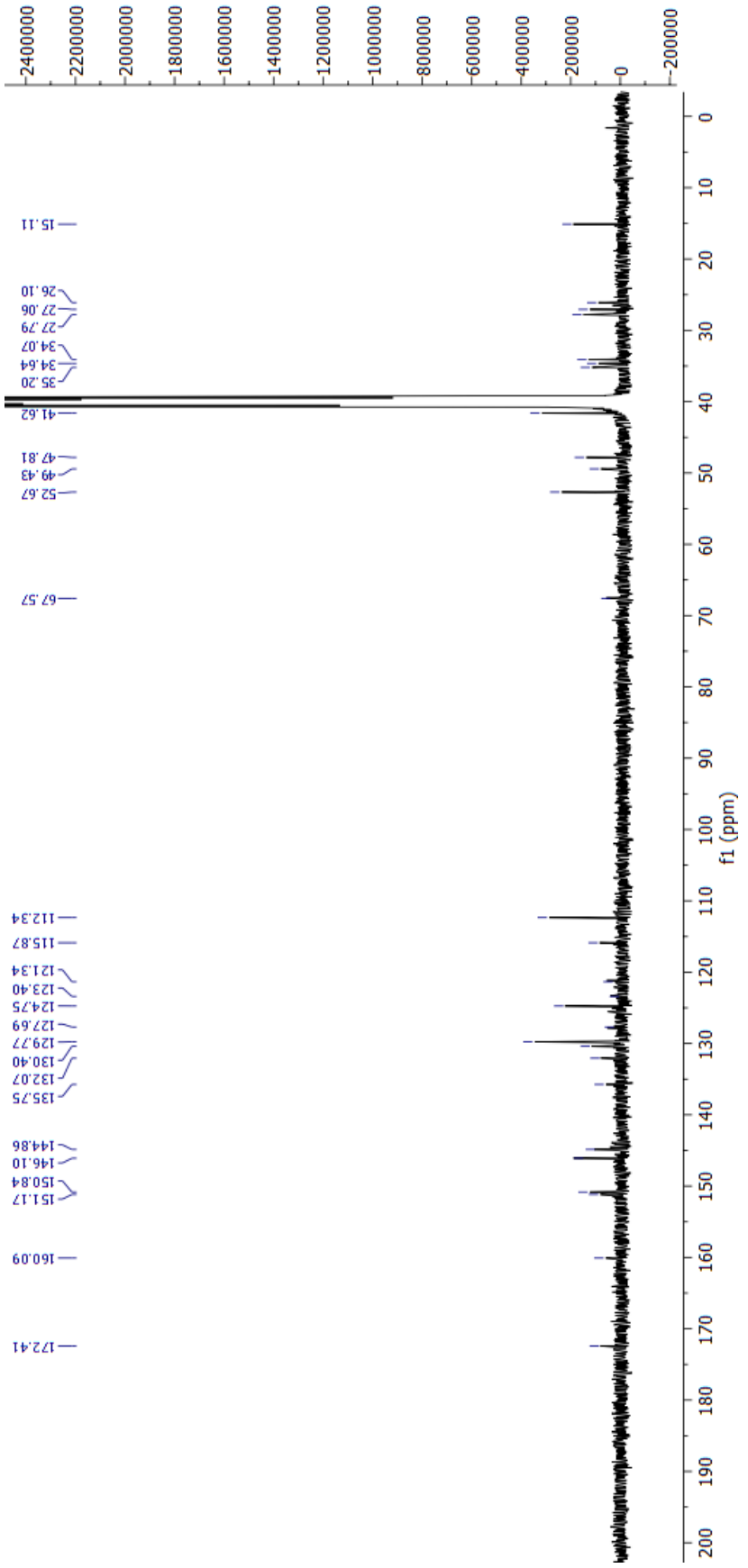

Appendix-6 HRMS Spectrum of compound L1

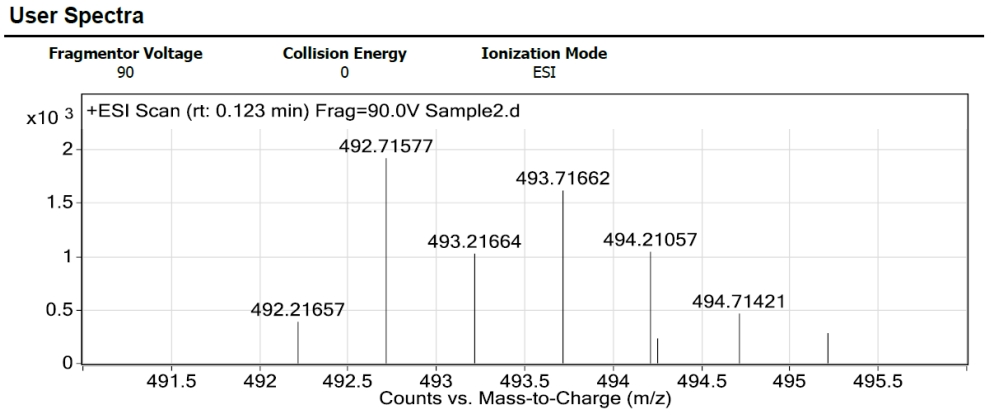

Appendix-7 ^{1}H NMR spectrum of compound 8 (400 MHz, $CDCl_3$).

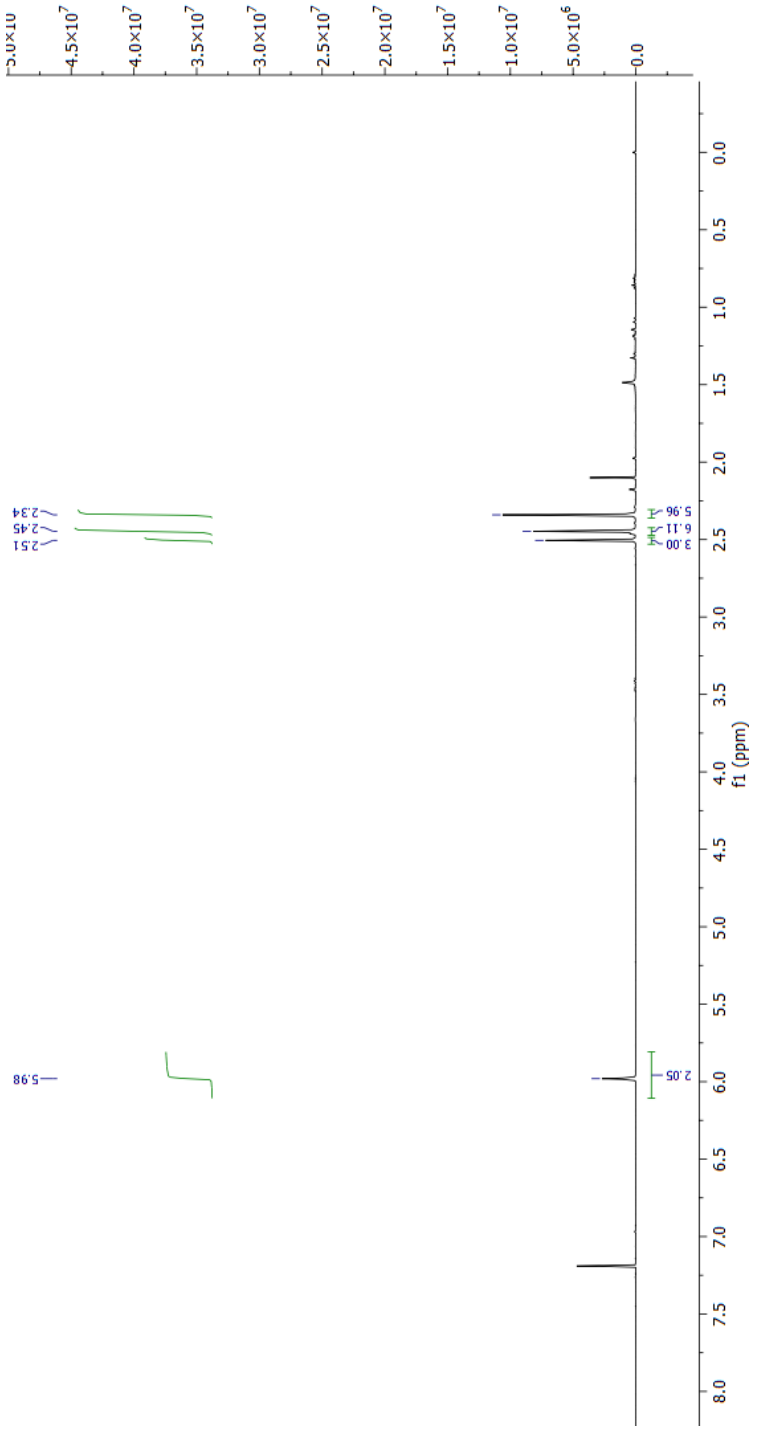

Appendix-8 ^{13}C NMR Spectrum of compound 8 (101 MHz, $CDCl_3$).

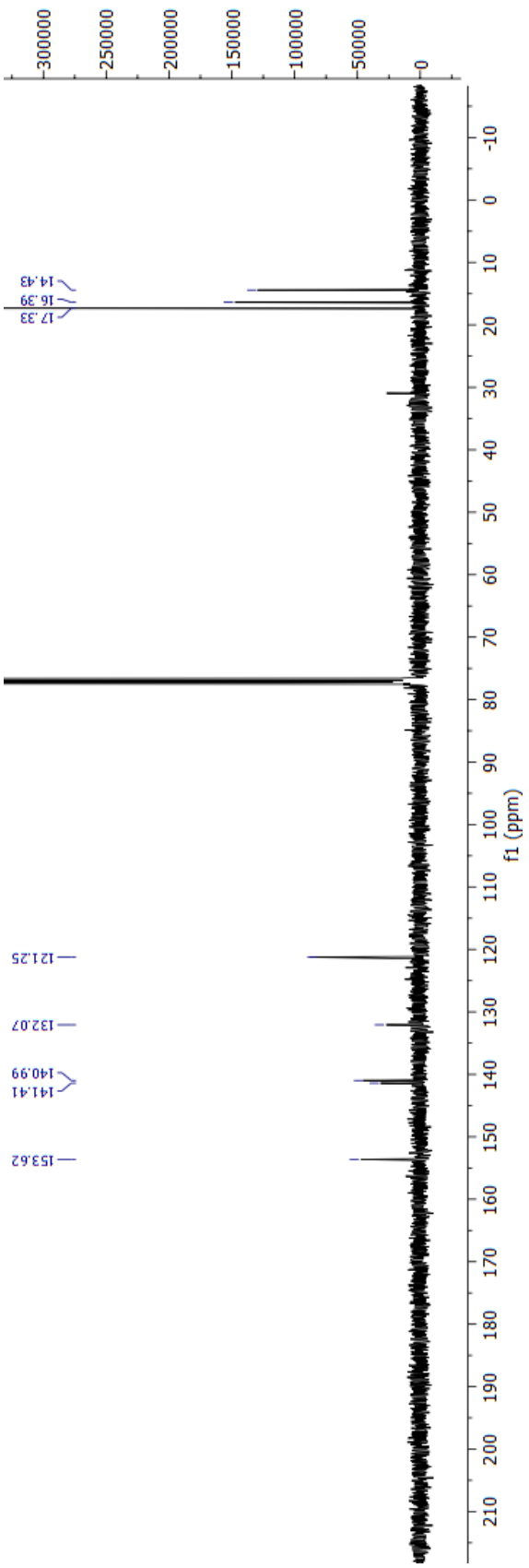

Appendix-9 HRMS Spectrum of compound 8

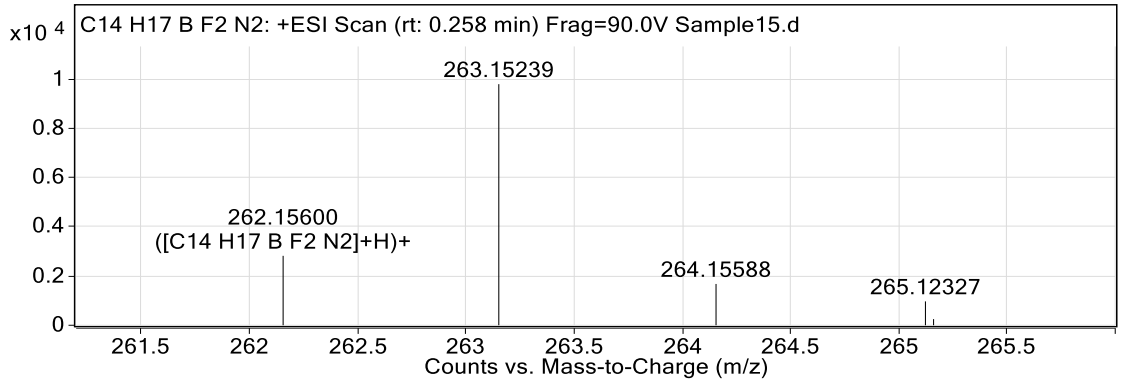

Appendix-10 ^{1}H NMR spectrum of compound 9 (400 MHz, $CDCl_3$).

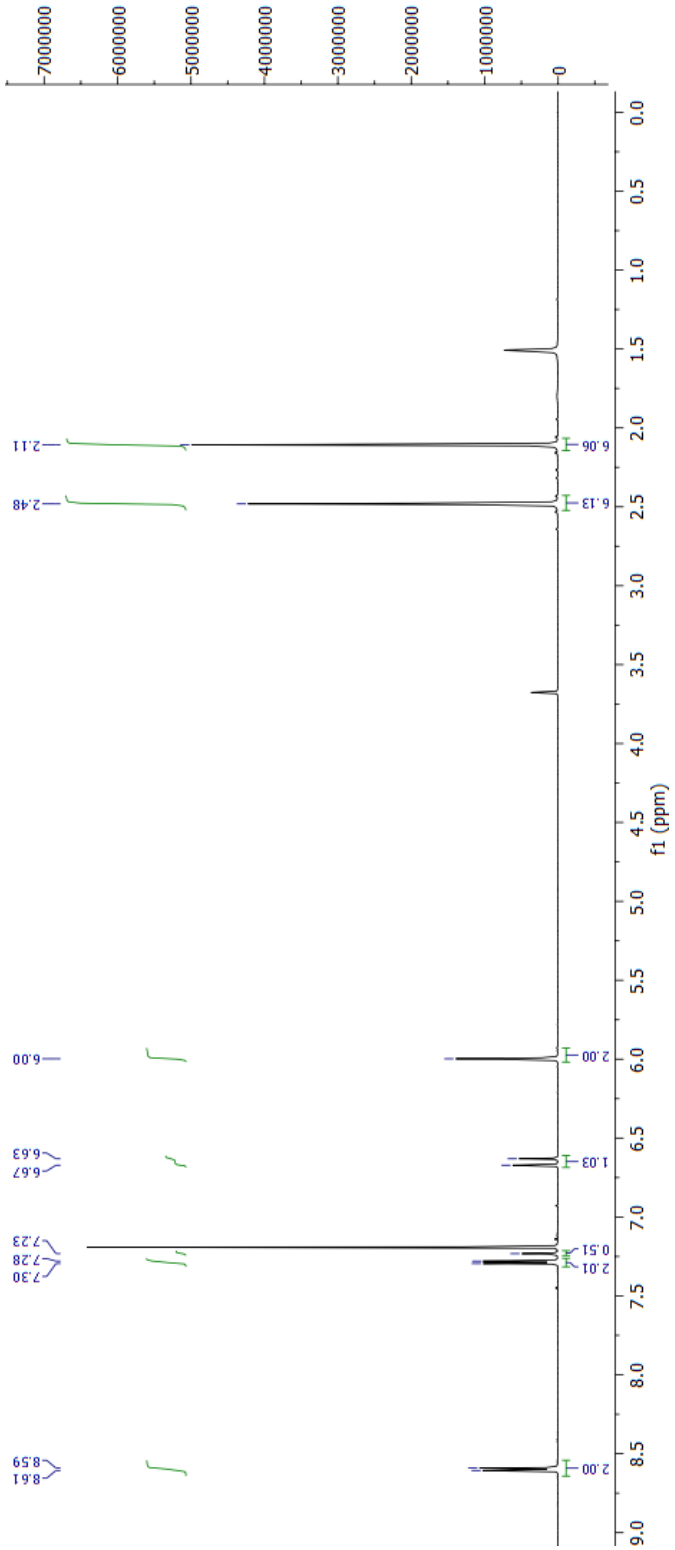

Appendix-11 ^{13}C NMR Spectrum of compound 9 (101 MHz, $CDCl_3$).

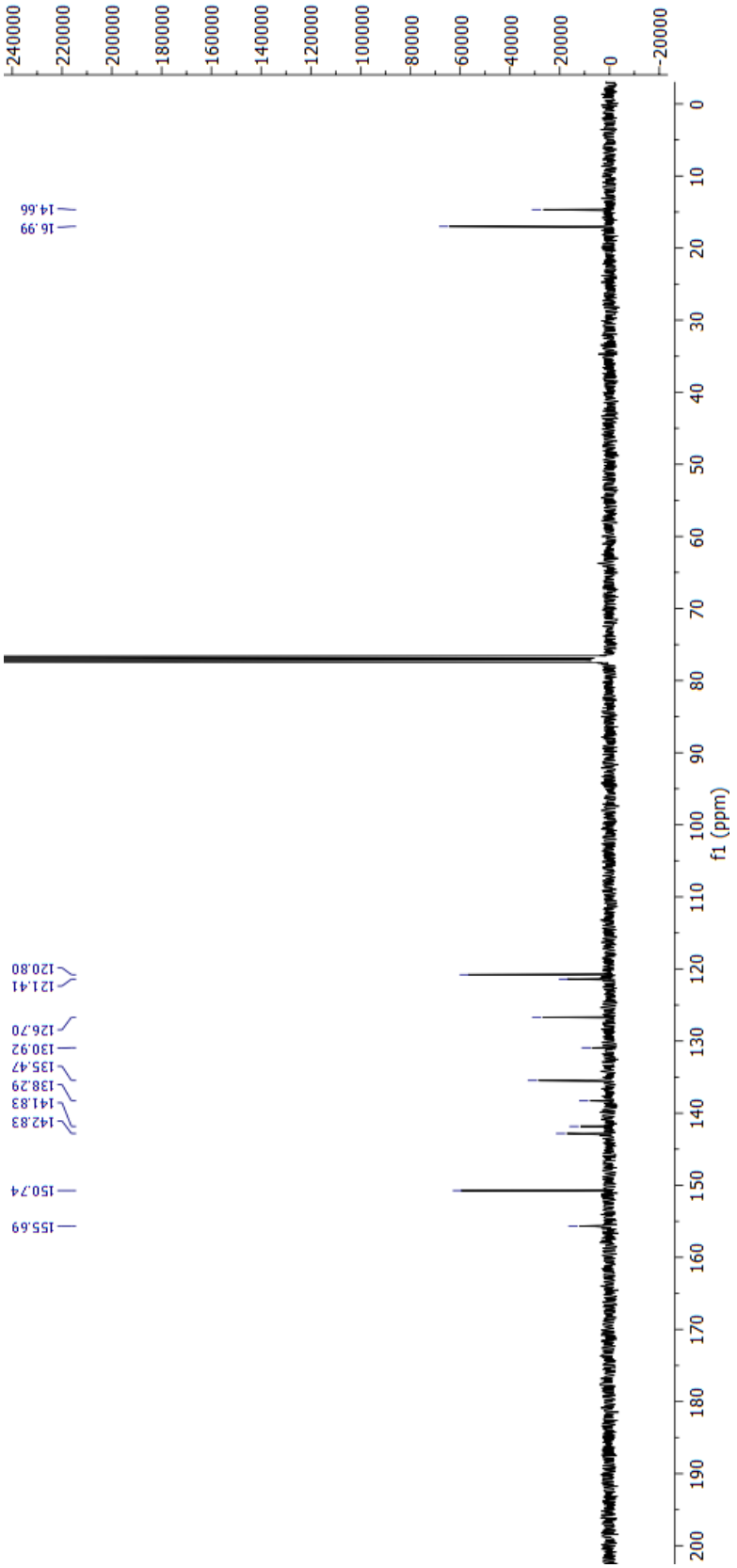

Appendix-12 HRMS Spectrum of compound 9

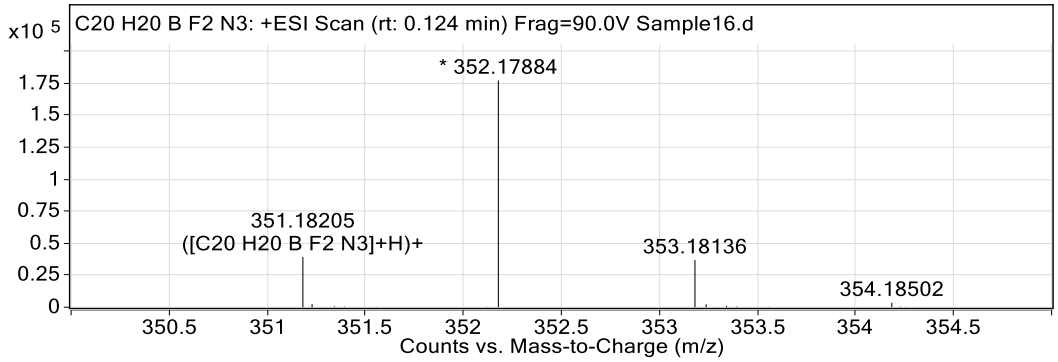

Appendix-13 ^{1}H NMR spectrum of compound 10 (400 MHz, $CDCl_3$).

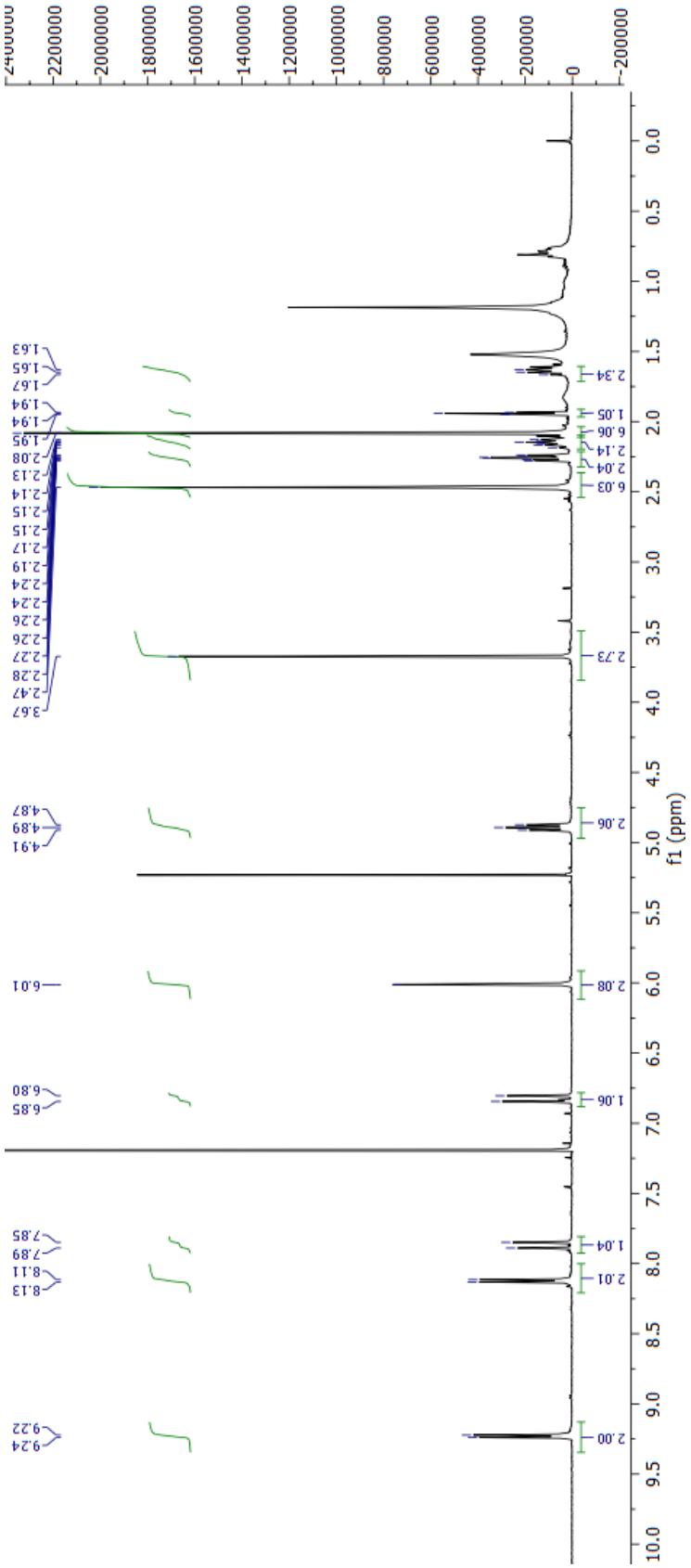

Appendix-14 ^{13}C NMR Spectrum of compound 10 (101 MHz, $CDCl_3$).

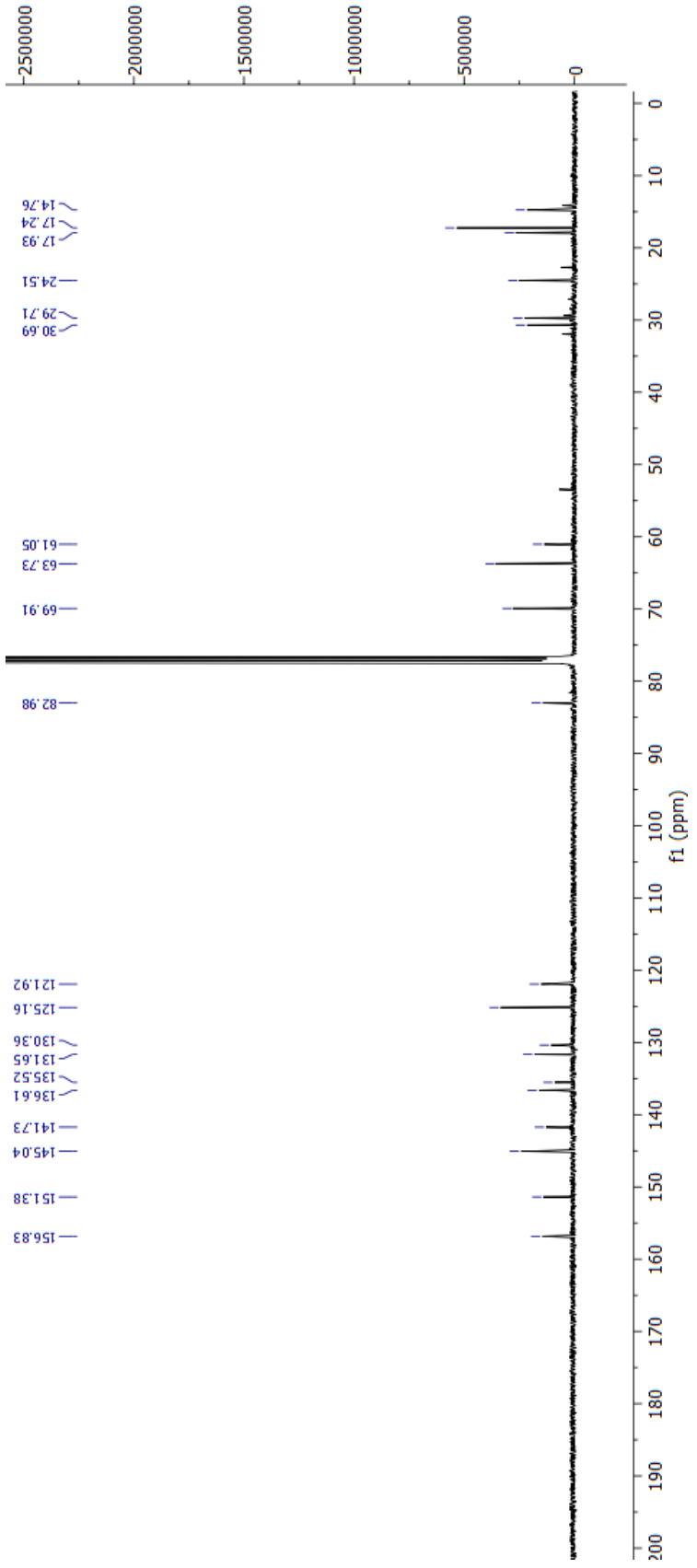

Appendix-15 HRMS Spectrum of compound 10

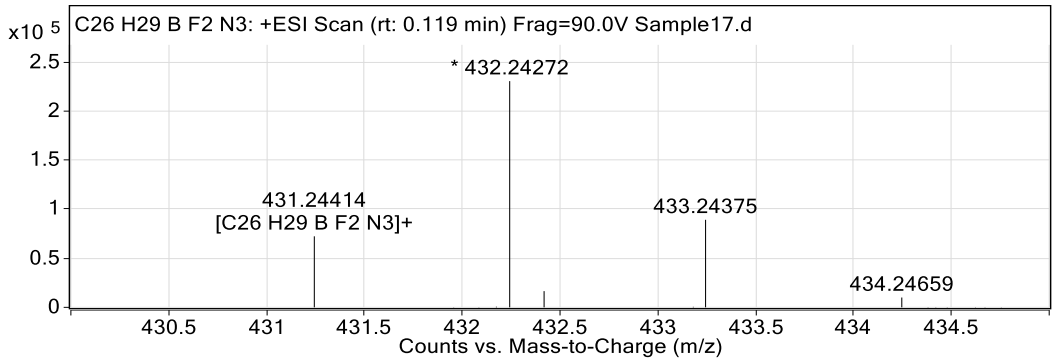

Appendix-16 ^{1}H NMR spectrum of compound 11 (400 MHz, $CDCl_3$).

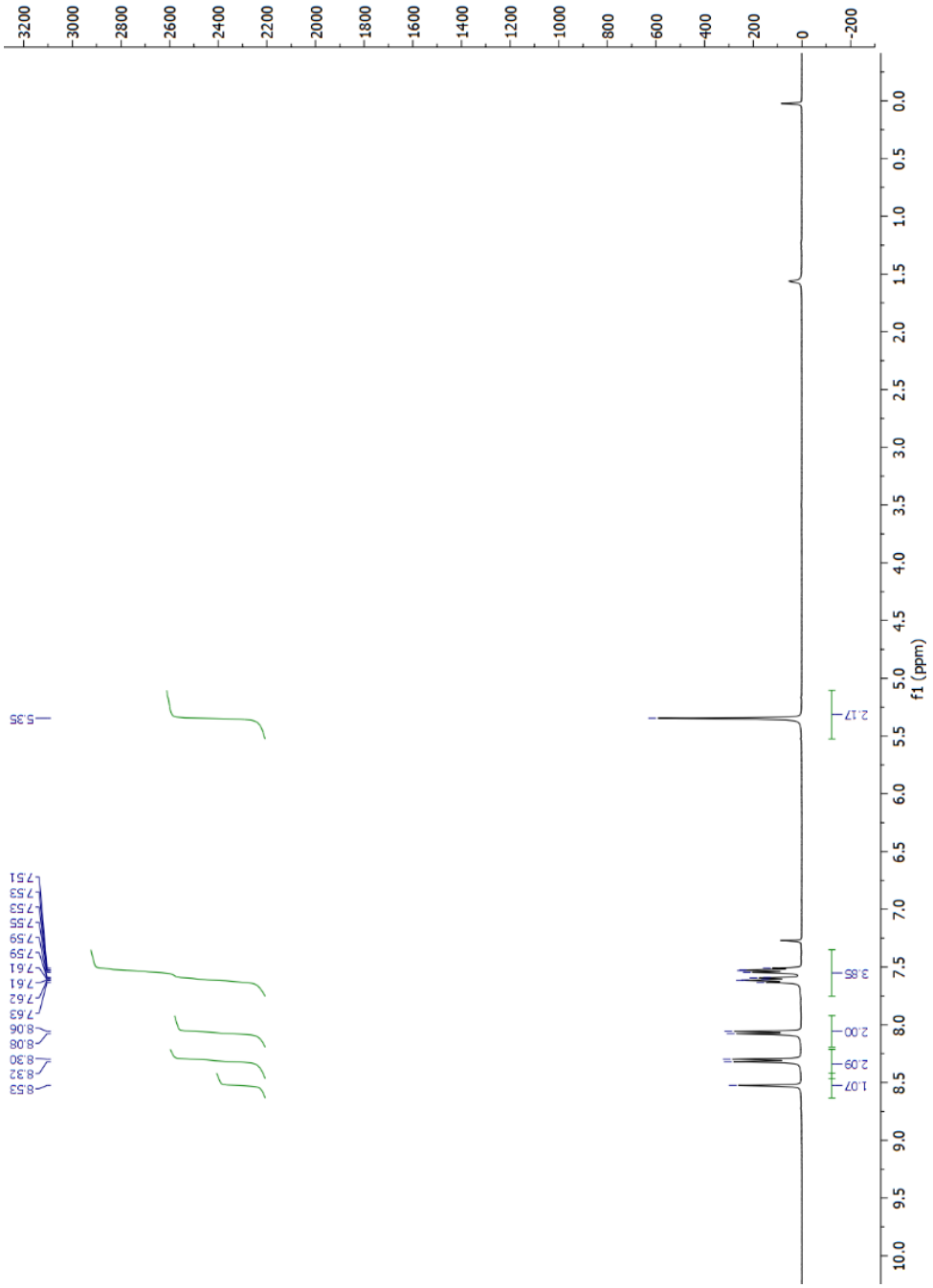

Appendix-17 ^{13}C NMR Spectrum of compound 11 (101 MHz, $CDCl_3$).

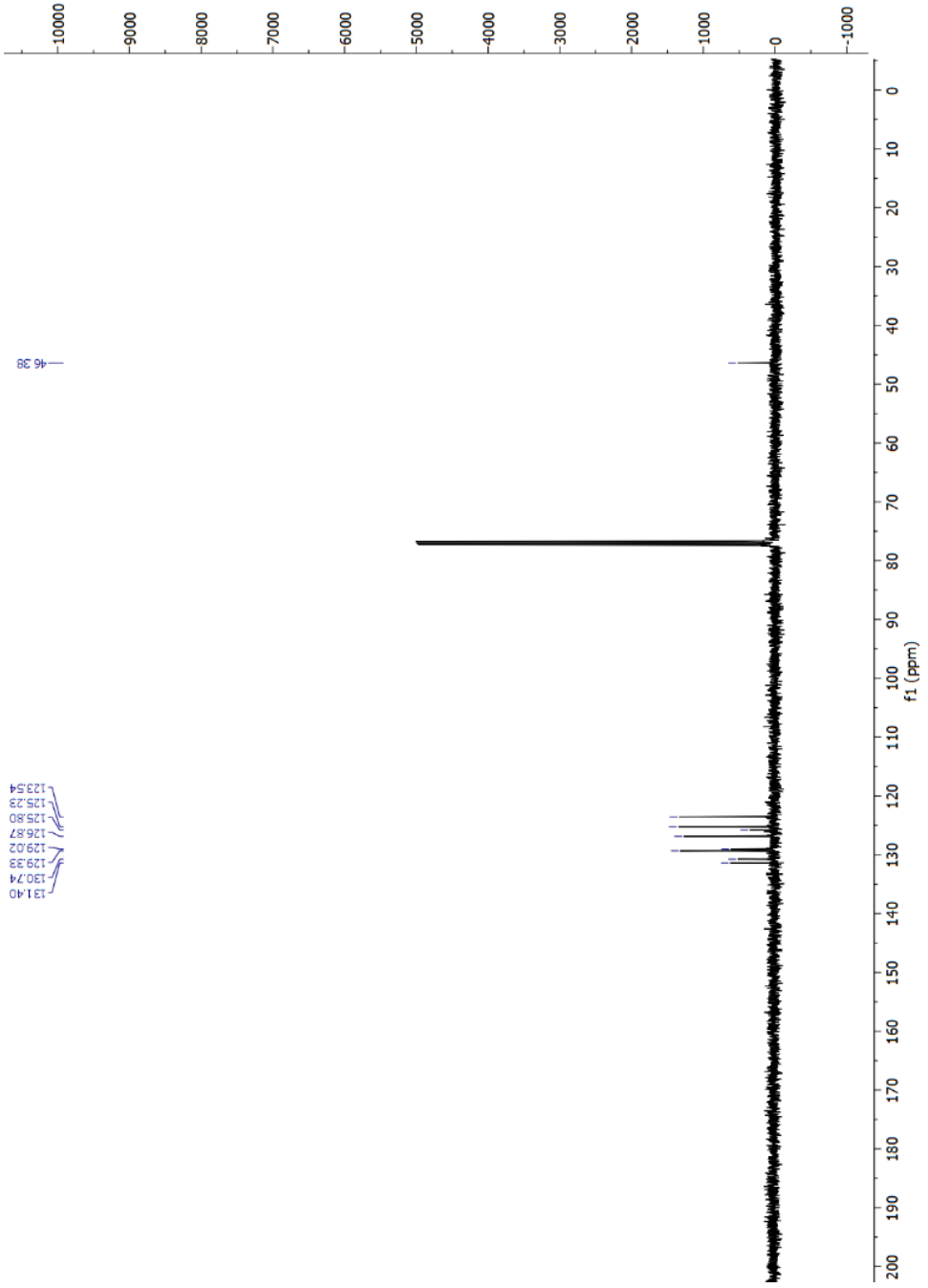

Appendix-18 HRMS Spectrum of compound 11

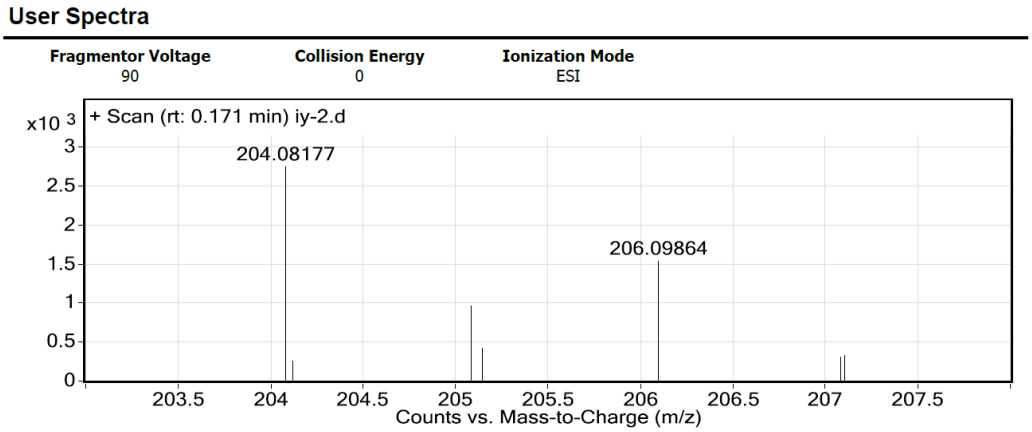

Appendix-19 ^{1}H NMR spectrum of compound 12 (400 MHz, $CDCl_3$).

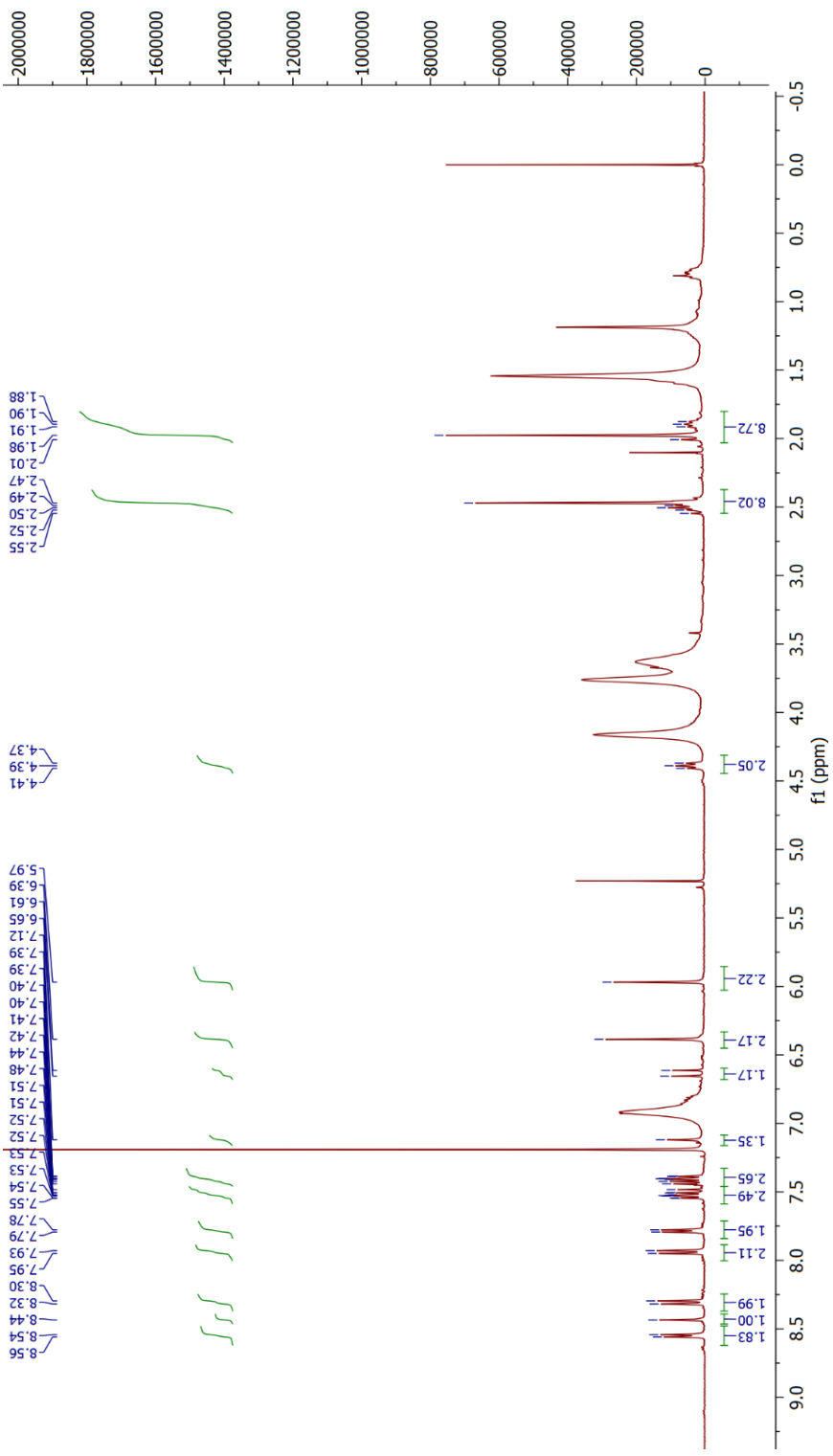

Appendix-20 HRMS Spectrum of compound 12

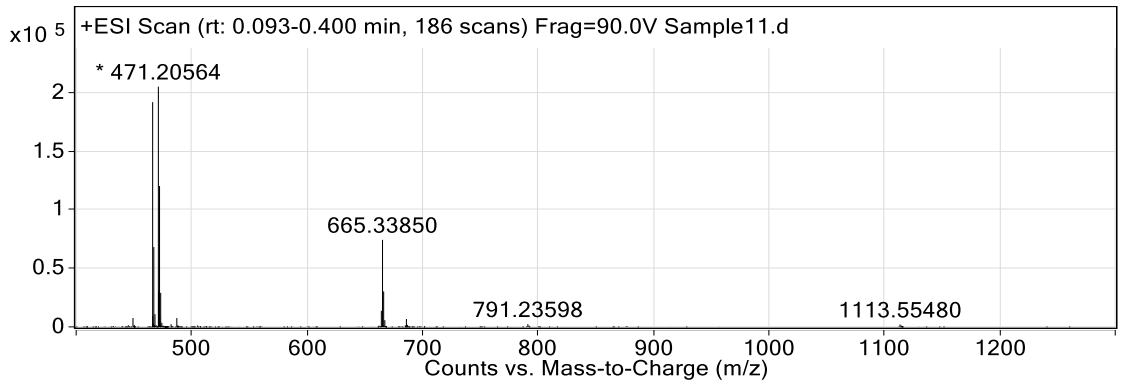

Appendix-21 ^{1}H NMR spectrum of compound L2 (400 MHz, $CDCl_3$

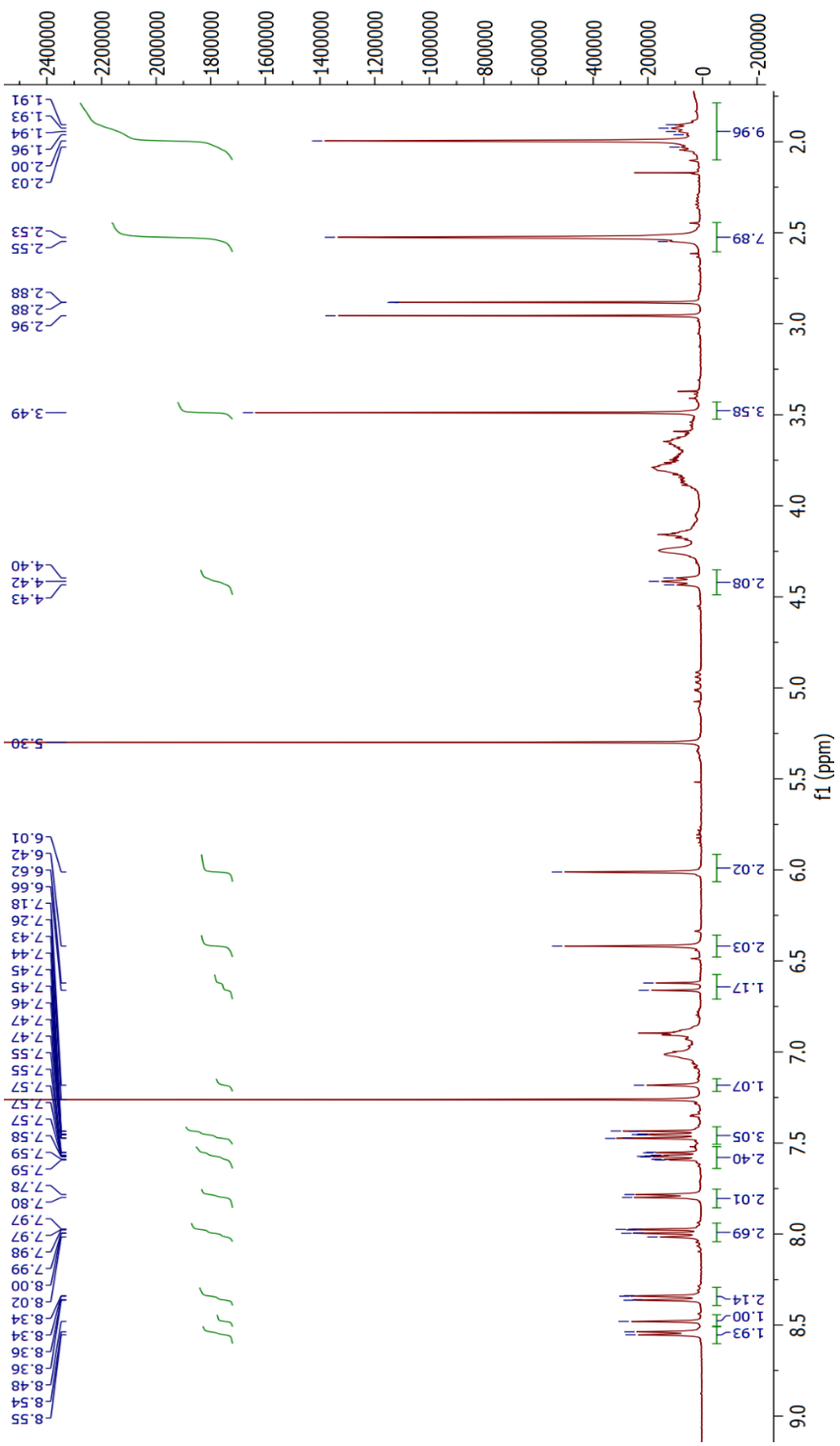

Appendix-22 HRMS Spectrum of compound L2